BBA - Biomembranes 1866 (2024) 184269

Contents lists available at ScienceDirect

BBA - Biomembranes

journal homepage: www.elsevier.com/locate/bbamem

^{19}F solid-state NMR approaches to probe antimicrobial peptide interactions with membranes in whole cells

Kiran Kumar [a], Alexandre A. Arnold [a], Raphaël Gauthier [b], Marius Mamone [b], Jean-François Paquin [b], Dror E. Warschawski [a,c,**], Isabelle Marcotte [a,*]

[a] Departement of Chemistry, Université du Québec à Montréal, P.O. Box 8888, Downtown Station, Montreal H3C 3P8, Canada
[b] PROTEO, CCVC, Département de chimie, Université Laval, 1045 Avenue de la Médecine, Québec, Québec G1V 0A6, Canada
[c] Laboratoire des Biomolécules, LBM, CNRS UMR 7203, Sorbonne Université, École normale supérieure, PSL University, 75005 Paris, France

ARTICLE INFO

Keywords:
Host defense peptides
Red blood cells
Lipid bilayer
Isotopic labeling
In-cell NMR
Model membranes

ABSTRACT

To address the global problem of bacterial antibiotic resistance, antimicrobial peptides (AMPs) are considered promising therapeutic candidates due to their broad-spectrum and membrane-lytic activity. As preferential interactions with bacteria are crucial, it is equally important to investigate and understand their impact on eukaryotic cells. In this study, we employed ^{19}F solid-state nuclear magnetic resonance (ssNMR) as a novel approach to examine the interaction of AMPs with whole red blood cells (RBCs). We used RBC ghosts (devoid of hemoglobin) and developed a protocol to label their lipid membranes with palmitic acid (PA) monofluorinated at carbon positions 4, 8, or 14 on the acyl chain, allowing us to probe different locations in model and intact RBC ghost membranes. Our work revealed that changes in the ^{19}F chemical shift anisotropy, monitored through a C—F bond order parameter (S_{CF}), can provide insights into lipid bilayer dynamics. This information was also obtained using magic-angle spinning ^{19}F ssNMR spectra with and without ^{1}H decoupling, by studying alterations in the second spectral moment (M_2) as well as the ^{19}F isotropic chemical shift, linewidth, T_1, and T_2 relaxation times. The appearance of an additional isotropic peak with a smaller chemical shift anisotropy, a narrower linewidth, and a shorter $T_{1,}$ induced by the AMP caerin 1.1, supports the presence of high-curvature regions in RBCs indicative of pore formation, analogous to its antimicrobial mechanism. In summary, the straightforward incorporation of monofluorinated FAs and rapid signal acquisition offer promising avenues for the study of whole cells using ^{19}F ssNMR.

1. Introduction

Antimicrobial resistance by disease-causing bacteria has become a global health threat with ensuing socioeconomic issues [1,2]. In recent decades, bacterial resistance has increased at an alarming rate, sustained by an extensive usage of antibiotics. There is thus an urgent need for alternative solutions to combat bacterial resistance and in this context, antimicrobial peptides (AMPs) and their mimics stand as promising antibiotic molecules. Indeed, their action mechanisms involving bacterial membrane disruption, damage to intracellular biomolecules and other oxidative damages [3], are nonspecific and thus hard to evolve against. Over 24,000 AMP sequences have been identified so far, both from natural and synthetic origins [4] and only a small number of AMPs or their mimics have reached clinical trials [5] or are already commercialized as antimicrobial agents (e.g. bacitracin, gramicidin D, polymyxin B) [5]. In vivo stability and low toxicity towards human cells are key factors to access the pharmaceutical market.

Since many AMPs target the bacterial lipid membrane, considerable

Abbreviations: AMP, antimicrobial peptide; CSA, chemical shift anisotropy; DPPC, dipalmitoylphosphatidylcholine; DPPC-d_{62}, perdeuterated dipalmitoylphosphatidylcholine; GC–MS, gas chromatography coupled to mass spectrometry; L/P, lipid-to-peptide; MAS, magic-angle spinning; MFFA, monofluorinated fatty acid; MLV, multilamellar vesicle; PA, palmitic acid; PA-F(4), (F8) or (F14), palmitic acid fluorinated at positions 4, 8 or 14; S/N, signal-to-noise; ssNMR, solid-state nuclear magnetic resonance; SSB, spinning sideband; T_m, melting temperature..

* Corresponding author at: Department of Chemistry, Université du Québec à Montréal, P.O. Box 8888, Downtown Station, Montreal H3C 3P8, Canada
** Corresponding author at: Laboratoire des Biomolécules, LBM, CNRS UMR 7203, Sorbonne Université, École normale supérieure, PSL University, 75005 Paris, France
E-mail addresses: Dror.Warschawski@Sorbonne-Universite.fr (D.E. Warschawski), marcotte.isabelle@uqam.ca (I. Marcotte).

https://doi.org/10.1016/j.bbamem.2023.184269
Received 27 September 2023; Received in revised form 19 December 2023; Accepted 21 December 2023
Available online 2 January 2024

efforts have been put into characterizing their interaction with cell membranes [6,7]. Solid-state NMR (ssNMR) has proved to be a unique tool to study such interactions at a nanoscopic level. Different NMR-active nuclei such as ^{1}H, ^{2}H, ^{13}C, and ^{31}P are used to study the biophysical properties of lipid membranes in the presence of AMPs [8–10]. Deuterium is mostly used to characterize lipid chain order and molecular events happening in the core of the bilayer environment, while phosphorus allows probing the lipid headgroups or assessing the overall topology of the lipid organization [11,12]. After some initial work on whole cells in the late 70s and early 80s, the field has heavily relied on model membranes until the early 2010s when our group and others reintroduced the use of whole-cell ^{2}H labelling [13–15]. Our laboratory has also developed the use of magic-angle spinning (MAS) combined to ^{2}H ssNMR to reduce the experimental time and ensure that cells remain intact [16].

^{19}F is an NMR-active nucleus with interesting properties, notably high sensitivity with low background in biological systems, strong dipolar couplings and a large chemical shift range. This sparked interest in its use to study native membranes already in the late seventies and early eighties, with papers showing that the incorporation of fluorinated fatty acid (FA) probes in native membranes was feasible [17,18]. Wild-type and auxotroph *Escherichia coli* strains were successfully labelled [19,20] as well as *Acholeplasma laidlawii* membranes [17], with FAs fluorinated at different positions, and with only weak perturbations to the membrane [17,19]. McDonough et al. [18] also showed that monofluorinated palmitic acids (H-C-F) had a less perturbing effect than difluorinated analogues (F-C-F), and also reported that a single fluorine atom in the bilayer was likely to have a less perturbing effect compared to bulkier electron spin or fluorescent probes. In all these studies, it was shown that an order profile along the acyl chains - similar to the one obtained by ^{2}H ssNMR - could be determined using ^{19}F ssNMR. However, except for one application from the group of Auger [21,22], the use of ^{19}F ssNMR has not been extensively developed to study AMP interactions *from a membrane point of view*. Indeed, the high sensitivity and almost complete absence of this nucleus in nature has stemmed a significant body of work on fluorinated peptides [23–26], but not on fluorinated membranes.

Early work on ^{19}F-labelled membranes either by a fluorinated fatty acid or phospholipid focused on static (no magic-angle spinning, MAS) samples and without ^{1}H decoupling [17–20,27]. The order profile in the acyl chains was, however, shown to be accessible and described by order parameters obtained through spectral fitting and normalizing by a rigid linewidth. More recently, ^{19}F-labelled phospholipids synthesis was achieved and these lipids were incorporated into model membranes [22,28–31]. ^{19}F positions spanning the whole acyl chain length and showed by ^{19}F ssNMR that the ^{19}F chemical shift anisotropy (CSA) decreased monotonically from the headgroup to the end of the acyl chain, thus informing on motion throughout the membrane. They also reported the strong ^{19}F isotropic chemical shift variation along the acyl chain. Protons were decoupled, but MAS was not used in this study.

^{19}F NMR thus appears as an excellent candidate to investigate membrane-AMP interactions in intact cells. In this work, we reintroduce the use of monofluorinated FAs (MFFAs) to label intact red blood cell (RBC) membranes and establish a ^{19}F ssNMR approach to study AMP-membrane interactions. More specifically, we incorporated into erythrocyte ghosts MFFAs labelled at positions 4, 8 and 14 on the acyl chains (Fig. 1A). Ghosts are erythrocytes from which hemoglobin has been removed, thus reducing potential interference of the paramagnetic heme group with NMR signals. After an initial assessment on a model membrane, we show how both in-cell static and MAS ^{19}F ssNMR can be

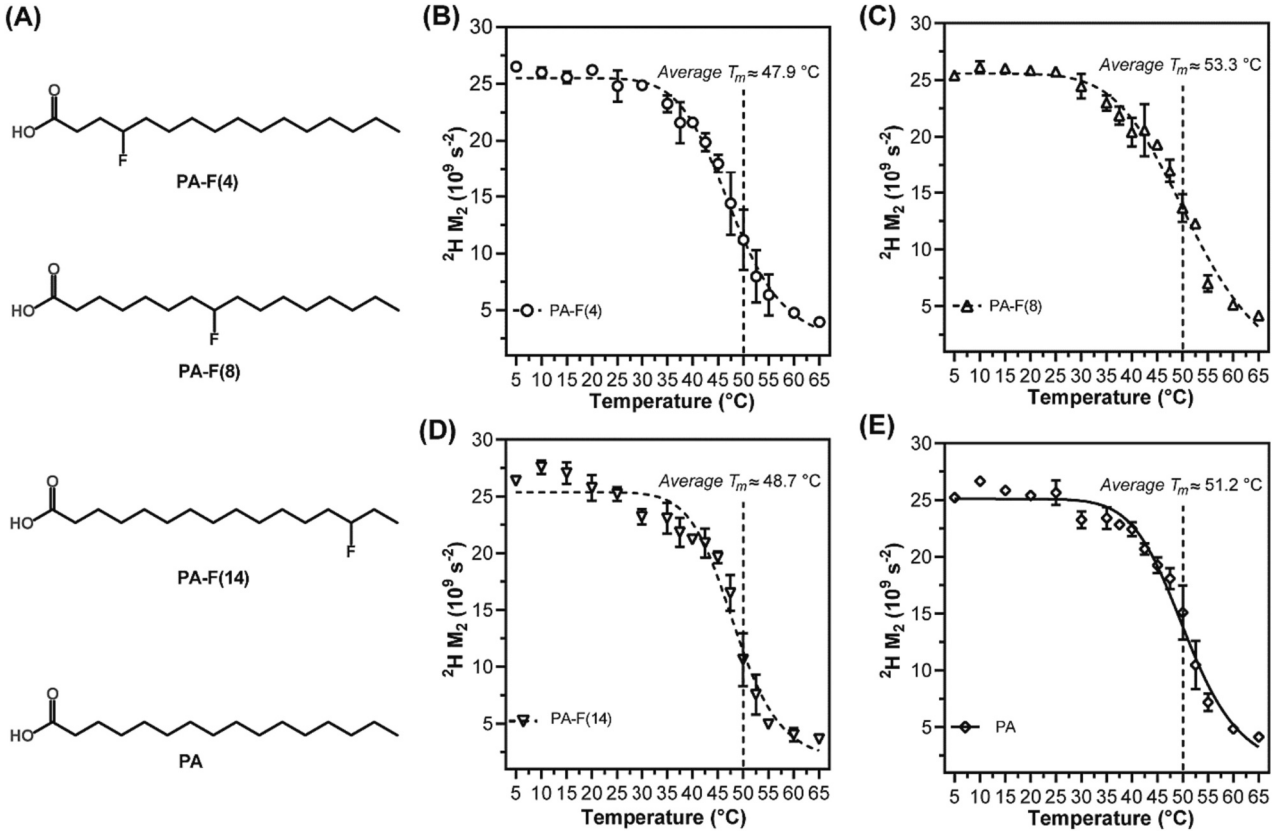

Fig. 1. Effect of fluorination on DPPC-d_{62}/PA model membranes. (A) PAs were fluorinated at different positions along the acyl chain. Second spectral moment (M_2) as a function of temperature. M_2 values were obtained from the ^{2}H ssNMR MAS spectra (Fig. S1) of DPPC/DPPC-d_{62}/PA at a molar ratio of (1:1:1) with fluorinated and non-fluorinated PA analogues, (B) with PA-F(4), (C) PA-F(8), (D) PA-F(14) and (E) PA. M_2 reports on acyl chain order and values are indicated with standard deviations.

exploited to study the pore formation mechanism of AMPs using caerin 1.1 - a natural AMPs isolated from the skin secretions of Australian tree frogs as a model.

2. Materials and methods

2.1. Materials

Caerin 1.1 was purchased from GenScript Corporation (Piscataway, NJ, USA) with >98 % purity. Protonated and deuterated dipalmitoylphosphatidylcholine (DPPC and DPPC-d_{62}) were obtained from Avanti Polar Lipids (Alabaster, AL, USA). Ethylenediaminetetraacetic free acid (EDTA) was bought from Fisher Scientific (Fair Lawn, NJ, USA), while unlabelled palmitic acid, deuterium-depleted water, Triton X-100, fatty acid methyl ester mix C4-C24 (FAME mix), [16-[(7-nitro-2-1,3-benzoxadiazol-4-yl)amino] palmitic acid (NBD-PA), 1,1′-dilinoleyl-3,3,3′,3′-tetramethylindocarbocyanine 4-chlorobenzenesulfonate (Fast DiI) and all other solvents and chemicals were purchased from Sigma Aldrich (Oakville, ON, Canada). Fresh horse RBCs packed 100 % were purchased from Cedarlane Laboratories (Burlington, ON, Canada). Deionized 18.2 MΩ.cm Milli-Q water was used in all experiments (Millipore-Sigma, Oakville, ON, Canada). Fluorine-labelled fatty acids were synthesized following a protocol detailed in the SI section.

2.2. Multilamellar vesicles (MLVs) preparation

MLVs were prepared using dry film method as described by Warschawski et al. [32]. The lipid mixture (including ^{19}F-labelled PAs) was dissolved in 1:2 methanol/$CHCl_3$ solution and dried under nitrogen stream. Remaining traces of organic solvent in the lipid film were removed by high vacuum for at least 2 h. The lipid film was then hydrated with a physiologically-relevant solution of 150 mM NaCl (pH 7.0) prepared with ^{2}H-depleted water. The lipid dispersion was vortexed and freeze-thawed 3 to 5 times (10 min at −20 °C, followed by 10 min above 40–55 °C) and transferred directly into a 4-mm rotor.

2.3. Preparation of ^{19}F-labelled erythrocyte ghosts

Erythrocyte ghosts were prepared as described by Kumar et al. [9]. Briefly, 3–4 mL of concentrated horse RBCs were suspended in a 40 mL round bottom centrifugation tube with 25 mL isotonic HEPES buffer (20 mM HEPES, 150 mM NaCl, pH 7.4), and centrifuged at 500*g* for 5 min at 4 °C. Then three supplementary washes were done with the same buffer until the supernatant became clear. After the final wash, the pellet was resuspended in 20 mL hypotonic HEPES buffer (20 mM HEPES, pH 7.4) and centrifuged at 25,000*g* for 40 min at 4 °C (rotor JA-20, Beckman). The supernatant was then removed, and the pellet transferred into new centrifuge tubes, leaving behind the "red button" that contains proteases. Additional washes (3 to 4) with the same buffer were carried out to obtain a hemoglobin-free white ghosts pellet.

A mixed micelles solution of 0.5 mM Triton X-100/0.25 mM of ^{19}F-labelled PA in isotonic buffer was prepared in a sealed glass vial with three freeze (−20 °C)/thaw (95 °C)/vortex shaking cycles. The white ghost pellet was then resuspended in 320 mL isotonic buffer to which 80 mL of the mixed micelles solution were transferred, and incubated for 15 min at 37 °C. The mixture of ghosts and micellized ^{19}F-labelled PA was then centrifuged at 25,000*g* for 20 min at 4 °C in different 20 mL aliquots. The excess detergent was washed away twice by centrifugation in isotonic buffer at 25,000*g* for 20 min at 4 °C. The ghost pellets were pooled together in a 1.5 mL Eppendorf tube and centrifuged at 20,000*g* for 20 min at 4 °C. The pellet was then washed with an isotonic buffer and centrifuged at 100,000*g* and 4 °C for 20 min. This concentrated pellet was collected and stored at 4 °C prior to the experiments and used within 3–4 days.

2.4. Sample preparation for confocal microscopy

A total of 1 % (v/v) of ^{19}F-labelled ghosts were labelled with the fluorophore Fast-DiI (1/1000) using a 1 h incubation at 37 °C, followed by pelleting at 16,000 g for 15 min, or with NBD-PA directly incorporated into ghosts along with ^{19}F-labelled PA as described above in Section 2.3. The pellet was resuspended in 500 μL of HEPES buffer then transferred to Sarstedt 8-well microscopy slides (300 μL) and left to stand for 30 min to allow ghosts immobilization. Samples were incubated for 1 h at 37 °C after addition of an appropriate amount of caerin 1.1 into 1 % (v/v) ghosts, and single frame per second images were generated using a Nikon confocal microscope with a 60× oil-immersion lens. Images were processed using ImageJ software.

2.5. Fatty acid profile and labelling efficiency

FA analyses were carried out using gas chromatography coupled to mass spectrometry (GCMS) as described by Laydevant et al. [33] following lipid extraction and transesterification. Briefly, lipids were extracted (triplicates) using the Folch protocol [14], then transesterified using 2 mL of H_2SO_4 (2 % in methanol) and 0.8 mL of toluene for 10 min at 100 °C. A polar HP-5MS column (30 m length × 250 μm diameter × 0.25 μm film thickness) was used with an injection volume of 1 μL, and the oven temperature was programmed to heat at 140 °C for 5 min followed by a 4 °C/min ramp up to 300 °C, prior to electron ionization and detection with a Agilent quadrupole MS. Data acquisition and processing were done with the Chemstation software.

2.6. Solid-state NMR and spectral analysis

All ssNMR spectra were recorded using a Bruker Avance III-HD wide-bore 400 MHz spectrometer (Milton, ON, Canada) equipped with a double tuned 4 mm-HFX probe and a ^{1}H—^{19}F filter. Static ^{19}F and ^{31}P ssNMR spectra were obtained using a phase-cycled Hahn echo pulse sequence, with an inter pulse delay of 35 μs and high-power (50 kHz) ^{1}H decoupling during acquisition. The 90° pulse length was 4 μs for ^{19}F ssNMR and 3 μs for ^{31}P ssNMR. Data were collected using 2048 points for ^{19}F ssNMR and 1024 points for ^{31}P ssNMR. The recycle delay was 2 s for ^{19}F ssNMR and 3 s for ^{31}P ssNMR. A total of 12 k scans per ^{19}F spectra for ghosts and 1 k scans for MLVs were collected, amounting to 7 h of acquisition for ghosts and 35 mins for MLVs. And a total of 14 k scans per ^{31}P spectra for ghosts and 1 k scans for MLVs were collected, amounting to 12 h of acquisition for ghosts and 50 mins for MLVs. The ^{31}P chemical shifts were referenced to the phosphoric acid (H_3PO_4) signal at 0 ppm, while the ^{19}F chemical shifts were referenced to the trifluoroacetic acid (TFA) signal at −76.5 ppm.

^{2}H and ^{19}F ssNMR experiments were also carried out at 10 kHz MAS frequency. A phase-cycled Hahn echo sequence was used for both MAS ^{2}H ssNMR experiments with MLVs samples and MAS ^{19}F ssNMR analysis of ghosts. ^{2}H ssNMR spectra were recorded with 100 k data points, a 4 μs 90° pulse length, rotor-synchronized interpulse delay of 96 μs and recycle time of 500 ms. A total of 1024 scans per spectra were collected, amounting to 8 min acquisition time. ^{19}F ssMAS spectra were collected with 3 k data points, a 4 μs 90° pulse length, rotor-synchronized interpulse delay of 94 μs and recycle time of 2 s. In model membrane sample a total of 512 scans per spectra were collected, amounting to 18 min of acquisition time with a recycle time of 2 s and in ghost sample a total of 6 k scans per spectra were collected, amounting to 3.5 h of acquisition time with a recycle time of 2 s.

^{31}P and ^{19}F CSA values were determined by line fitting using the Bruker Topspin 4.0.6 software with Sola (Solid Lineshape Analysis) program and values from minimum two replicates are reported. Since the CSA is proportional to the order parameter, a bond order parameter S_{CF} was calculated using Eq. (1) [19]. The ^{19}F CSA measured on pure and dry fluorinated PAs at −30 °C was taken as the rigid CSA (≈18 ppm):

$$S_{CF} = \frac{Observed^{19}F\ CSA}{Rigid^{19}F\ CSA} \quad (1)$$

^{2}H spectral moment analysis was performed using MestRenova software V6.0 (Mestrelab Research, Santiago de Compostela, Spain). Second spectral moments, M_2, were calculated using Eq. (2) [34,35] and values from minimum two replicates are reported.

$$M_2 = \omega_r^2 \frac{\Sigma_{N=0}^{\infty} N^2 A_N}{\sum_{N=0}^{\infty} A_N} = \frac{9\Pi^2 \chi_Q^2}{20} \langle S_{CD}^2 \rangle \quad (2)$$

where ω_r is the angular spinning frequency, N is the side band number, and A_N is the area of each sideband obtained by spectral integration, S_{CD}^2 is the mean square order parameter, and χ_Q is the static quadrupolar coupling constant equal to 168 kHz for a C—D bond in acyl chains. The M_2 value provides a quantitative description of the membrane lipid ordering and is particularly sensitive to the gel-to-fluid phase transition. In the case of ^{19}F ssNMR, M_2 can also be determined using the first part of Eq. (2).

3. Results

3.1. Fluorinated FAs as reporters of membrane structure and order

FAs are molecular probes that can be readily incorporated into biological membranes to study their biophysical properties in native cellular conditions [9]. The incorporation of exogenous FAs into living cells is often easier than other labelling strategies exploiting the cell's biochemistry [36,37]. Moreover, free FAs are natural constituents of cell membranes where they are involved in various cellular processes and play a role in regulating cellular functions and membrane fluidity [38]. However, incorporating high concentrations of FAs can change the bilayer phase behavior - an effect that has been addressed in previous works [39–42]. For example, the gel (L_β)-to-fluid (L_α) phase transition temperature (T_m) of a lipid membrane is increased by the presence of FAs, and a coexistence of gel and fluid phases can occur at certain phospholipid/FA ratios [41]. Nevertheless, FAs remain accurate reporters of variations in the lipid order in a membrane system [41]. Therefore, before incorporating MFFAs in whole cells' membranes, we characterized their effect on the membrane fluidity and as a function of the fluorine atom position on the acyl chain.

We used model dipalmitoylphosphatidylcholine (DPPC) membranes to assess the effect of palmitic acid (PA) fluorinated at positions 4, 8 or 14, referred to as PA-F(4), PA-F(8) and PA-F(14) (Fig. 1A). The addition of perdeuterated DPPC (DPPC-d_{62}) allowed monitoring the membrane order profile by measuring the variation of the second spectral moment (M_2) calculated from ^{2}H ssNMR spectra as a function of temperature, as described elsewhere [16,43]. Examples of such spectra, can be found in Fig. S1.

The DPPC/PA mixture results in a complex phase diagram in which, at intermediate temperatures, PA-rich gel and DPPC-rich fluid phases coexist [42]. As shown in Fig. 1B to E, the order profile as well as T_m of DPPC varies very little when comparing fluorinated and non-fluorinated samples. The average T_m determined by ^{2}H ssNMR is centered at ≈ 48–53 °C. Our results are consistent with previous studies of the phase behavior of PA-containing DPPC bilayers [39,42]. In their investigation of the pseudo-binary phase diagram of DPPC/PA mixtures, Inoue et al. [42] reported a $T_m \sim$ 53–54 °C at 2:1 DPPC/PA molar ratio. The melting of the acyl chain can also be monitored using the ^{1}H ssNMR intensity of the main-chain CH_2 peak, as well as other lipid resonances (Fig. S2). In this case, T_m is centered at ~53–54 °C (Fig. S3) - a difference expected between protonated and deuterated phospholipid analogues [44]. Overall, our results show that the insertion of one fluorine atom in the bilayer (positions 4, 8 and 14 on PA acyl chain), has a very weak perturbing effect.

The pioneering work on ^{19}F-labelled biological membranes from the late 70's and early 80's was technically limited to non-spinning samples and ^{19}F detection without ^{1}H decoupling. The single recent work on membranes labelled with monofluorinated phospholipids carried out by Gagnon et al. [22] showed that, with ^{1}H decoupling, the ^{19}F lineshape could be used to assess the local order at a given acyl chain position. They also reported a strong ^{19}F isotropic chemical shift difference along the phospholipid acyl chains - a property that could be exploited to determine the acyl chain order in multiply labelled FAs or lipids using MAS. In their study, similarities are observable between ^{31}P and ^{19}F lineshapes, indicating that ^{19}F could be exploited in a similar fashion to ^{31}P to study the formation of fast tumbling structures that can be induced by membrane-active AMPs [45]. This is notably the case of AMPs that act through a carpet mechanism [9,45].

We verified whether ^{19}F ssNMR spectra of model membranes labelled with MFFAs could reflect changes in membrane structure and acyl-chain local order. Fig. 2 compares the static ^{31}P and ^{19}F ssNMR spectra of DPPC membranes incorporating PA-F(4), PA-F(8) or PA-F (14). ^{31}P spectra indicate changes in the phospholipids headgroup dynamics while ^{19}F spectra probe the hydrophobic region of the bilayer. The ^{31}P spectra lineshapes in Fig. 2 are characteristic of lipids in a lamellar phase with axial symmetry, and clearly reveal a gel (L_β)-to-fluid (L_α) phase transition. For such systems, this transition can be quantified by measuring the chemical shift anisotropy (CSA), which value is related to the spectrum width and decreases with increasing molecular dynamics. As seen in Fig. 3A, characteristic gel phases were detected up to 30 °C with a ^{31}P CSA value of 36 ppm that gradually dropped to 25 ppm at 45 °C, as the first components of the bilayer reach their phase transition temperature. In comparison, we determined CSA of 36–40 ppm in pure DPPC/DPPC-d_{62} membranes (Fig. S4) at a gel phase (up to 25 °C), which gradually dropped to 29 ppm at the fluid phase (42 °C). The addition of protonated PA shifted T_m to ~45–50 °C, as expected from the DPPC-PA phase diagram [42].

^{19}F ssNMR lineshapes of the MFFAs show strong similarities with ^{31}P ssNMR spectra, in particular in the gel phase with powder patterns characteristic of multilamellar vesicles (Fig. 2). As shown in Fig. 3A, the change in CSA values through the gel-to-fluid phase transition is analogous to the one observed with ^{31}P ssNMR. The gel phase is maintained up to 25 °C with ^{19}F CSA values of 14–16.5 ppm, and a noticeable larger CSA of 16.5 ppm when the ^{19}F-label is on the 8th carbon position, indicating a higher degree of order at the center of the lipid monolayer. Although ^{19}F CSA values are smaller than those of ^{31}P, they are very sensitive to changes in membrane fluidity. Indeed, when transitioning from the gel to the fluid phase, ^{19}F CSA values are reduced by 87 % on average. Above 25 °C up to about 42 °C, a coexistence of gel and fluid phases is observed in the ^{19}F spectra (Fig. 2 and 3A-C), consistent with the DPPC-PA phase diagram [42]. In the fluid phase, the ^{19}F CSA values range from ~1 ppm (PA-F(14)) to 4 ppm (PA-F(4)), depending on the fluorine atom position. This result is in agreement with the conformation and order profile along the acyl chains, with position 4 close to the headgroup undergoing less *trans-gauche* isomerisations than the 14th position, closer to the terminal methyl group.

Positioning ^{19}F atoms at different places along the FA acyl chain enables assessing the local order of the bilayer's hydrophobic region, from the interface to the core [19,22,27]. Providing that FAs undergo fast rotational motion along their long axis, this order can be quantified by introducing an order parameter, which describes the dynamic reorientation of a bond with respect to the main axis. This parameter is obtained by normalizing a given NMR-measured quantity in a mobile segment by its value in the static case. In the case of ^{2}H ssNMR for example, this is the quadrupolar coupling for a static C—D bond [43].

In early ^{19}F ssNMR studies, spectra were recorded without ^{1}H decoupling; the CSA and dipolar couplings interactions could therefore not be isolated, and were estimated by computer-assisted line fitting [19,27]. When employing high-power ^{1}H decoupling, it is reasonable to assume that only the CSA persists, simplifying the determination of the order parameter [46]. Here, we introduced a C—F bond order

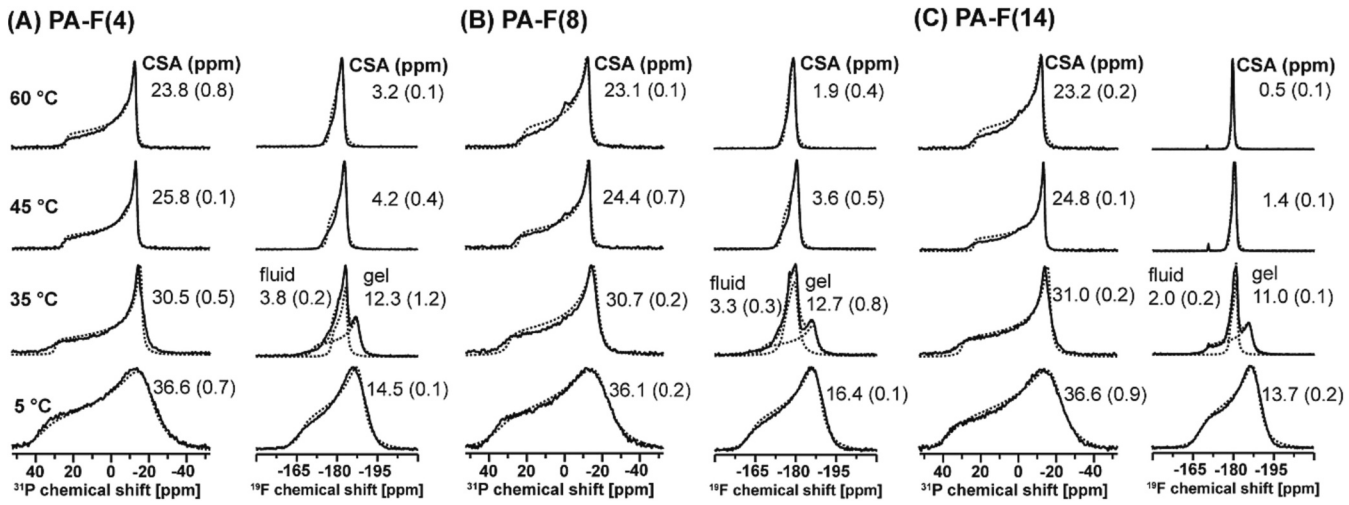

Fig. 2. Static ^{31}P and ^{19}F ssNMR spectra of DPPC model membranes incorporating monofluorinated PAs, at a DPPC/DPPC-d_{62}/PA molar ratio of 1:1:1 (A) with PA-F (4), (B) PA-F(8) and (C) PA-F(14). Experiments were performed at different temperatures with ^{1}H decoupling. Fitted spectra are shown as dashed lines. Average CSA values are indicated, with standard deviation.

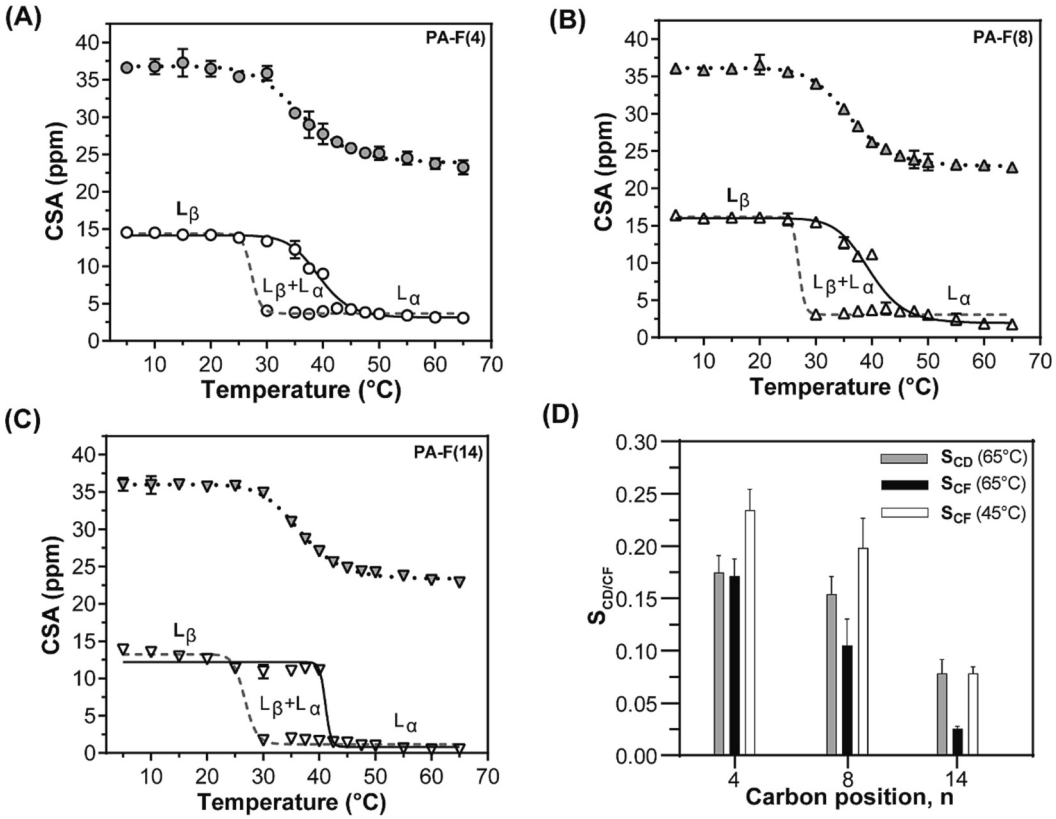

Fig. 3. Temperature dependence of the static ^{31}P (dotted lines) and ^{19}F (solid and dashed lines) CSA values for DPPC membranes with monofluorinated PAs at a molar ratio of 1:1, calculated from Fig. 2. (A) PA-F(4), (B) PA-F(8) and (C) PA-F(14) with filled symbols corresponding to ^{31}P ssNMR and empty ones to ^{19}F ssNMR. Note the presence of two components detected by ^{19}F ssNMR in the coexistence region. (D) ^{2}H (S_{CD}) and ^{19}F (S_{CF}) order parameter profile of the acyl chain in ^{19}F-labelled DPPC membranes as a function of the fluorine atom position, at 45 and 65 °C, with standard deviation.

parameter, S_{CF}, defined as the ratio between the experimentally-measured CSA and its value for an immobile C—F bond (Eq. (1)). By definition a rigid molecule with an all-*trans* conformation has an order parameter of $S_{CF} = 1$ while this value is 0 in the case of fast isotropic motions. The ^{19}F CSA tensor is not aligned along the C—F bond, and not necessarily axially symmetric, but in the fluid phase it becomes pseudo-axially symmetric with respect to the FA's long axis, as reflected in the spectra. Fig. 3D shows the S_{CF} bond order parameters for PA-F(4), -F(8) and -F(14) in model membranes. As a means of comparison, the S_{CD} order parameter of DPPC-d_{62} measured in the same sample is also presented (Fig. S5). The similarity of S_{CF} and S_{CD} values suggests that the relative orientation of the ^{19}F CSA tensor with respect to the molecular frame is factored out when the dry FA at −30 °C is used as the reference spectrum. The evolution of the two order parameters adequately reflect

dynamic changes with carbon position and temperature, confirming that the S_{CF} of MFFAs can be efficiently employed to measure the order profile along the acyl chains.

In the case of intact cells, measuring the acyl chain order at each carbon position is usually impossible. When perdeuterated lipids are used, the distribution of quadrupolar couplings, which reflects the overall dynamics in the membrane, can be assessed by measuring the second spectral moment, M_2, of the ^{2}H ssNMR spectra [43]. As we showed in a previous work, M_2 can also be determined under MAS conditions, which enhances the signal-to-noise (S/N) ratio and decreases the acquisition time [16]. Fig. 4 shows ^{19}F ssNMR spectra obtained in the gel and fluid states under 10 kHz MAS. The resulting increase in S/N ratio with respect to the static spectra is ca. ≈ 5–6-fold, corresponding to a reduction in acquisition time by a factor 25–36 for the same S/N ratio. This substantial gain in sensitivity enables recording spectra without ^{1}H decoupling (Fig. S6) - an important alternative considering that not all laboratories are equipped with probes capable of detecting ^{19}F while decoupling ^{1}H. Additionally, it allows working with significantly lower proportions of FAs in the membrane, as demonstrated in Fig. S7. At an MAS frequency of 10 kHz, the ^{19}F CSA (ranging between 0.3 kHz in the fluid phase and 6.5 kHz in the gel phase) should be entirely averaged out. Note that the CSA varies linearly with the static magnetic field strength, necessitating faster spin rates at higher fields. While spectra are dominated by an isotropic peak (δ_{iso}), 1–2 spinning sidebands (SSBs) are observed even in the ^{1}H-decoupled spectra albeit with lower intensity as compared to non-decoupled spectra. In principle, ^{1}H—^{19}F dipolar couplings should be eliminated by the strong ^{1}H decoupling, and the intermolecular ^{19}F—^{19}F dipole-dipole interactions significantly reduced by MAS. However, it is possible that residual dipolar couplings (^{1}H—^{19}F and/or ^{19}F—^{19}F) remain, or that internal acyl chain motions result in incomplete MAS averaging. In both cases, a change in membrane fluidity would lead to a corresponding alteration in the SSBs' intensities – as is indeed observed when temperature is varied. This feature can be exploited to assess the overall membrane dynamics, as will be shown below. It would be interesting to record the spectra at different magnetic fields in order to determine the relative contribution of field-dependent interactions, such as CSA, to the spinning sideband intensities.

The isotropic chemical shift (Table S1) is sensitive to the ^{19}F position on the FA chain, and also to the membrane lipid phase for positions 8 and 14 (Fig. 4 and Fig. S6). Indeed, two peaks are observed in the gel-fluid coexistence region (between 25 °C and 52 °C) separated by up to 0.8 ppm for these positions. The isotropic resonances are separated by up to 1.1 ppm between the gel (5 °C) and fluid (60 °C) phases (Fig. 4A). These peaks are easier to distinguish in the ^{1}H-decoupled spectra where they are almost baseline-resolved. As mentioned, the presence of SSBs allows measuring the ^{19}F spectral moment value (M_2), which reports on the membrane fluidity. Fig. 4B shows the evolution of M_2 as a function of temperature for both ^{1}H-coupled and decoupled spectra. Spinning sidebands were more intense when no decoupling was applied and the M_2 values varied between 38 × 10^6 s^{-2} in the gel phase down to 2–3 × 10^6 s^{-2} at 60 °C (fluid phase) for ^{19}F at positions 4 and 8. When the 14th carbon was ^{19}F-labelled (closer to the terminal methyl group) the M_2 value was smaller in the gel phase (25–32 × 10^6 s^{-2}) as compared to PA-F(4) and PA-(F8), but their M_2 values in the fluid phase were all very similar (2–3 × 10^6 s^{-2}). When ^{1}H decoupling was applied, the SSBs' intensity was significantly reduced, as previously mentioned. The M_2 values dropped to 6.8 and 11.7 × 10^6 s^{-2} in the gel phase for positions 8 and 14, respectively. In the fluid phase, the SSBs almost disappeared and the M_2 values were further reduced to 1 × 10^6 s^{-2}. Overall, our results show that M_2 values vary sufficiently between the gel and fluid phases for both ^{1}H-coupled and decoupled spectra to be used to assess membrane fluidity and detect phase transition temperatures. When feasible, we recommend recording the spectra with and without ^{1}H decoupling. In favorable cases, ^{1}H decoupling might allow determining the gel phase proportion by a simple integration of the isotropic lines since the ^{19}F isotropic chemical shift varies with membrane melting. On the other hand, the second spectral moment variation is larger on spectra without ^{1}H decoupling and membrane fluidity can thus be assessed from the M_2 with a higher precision.

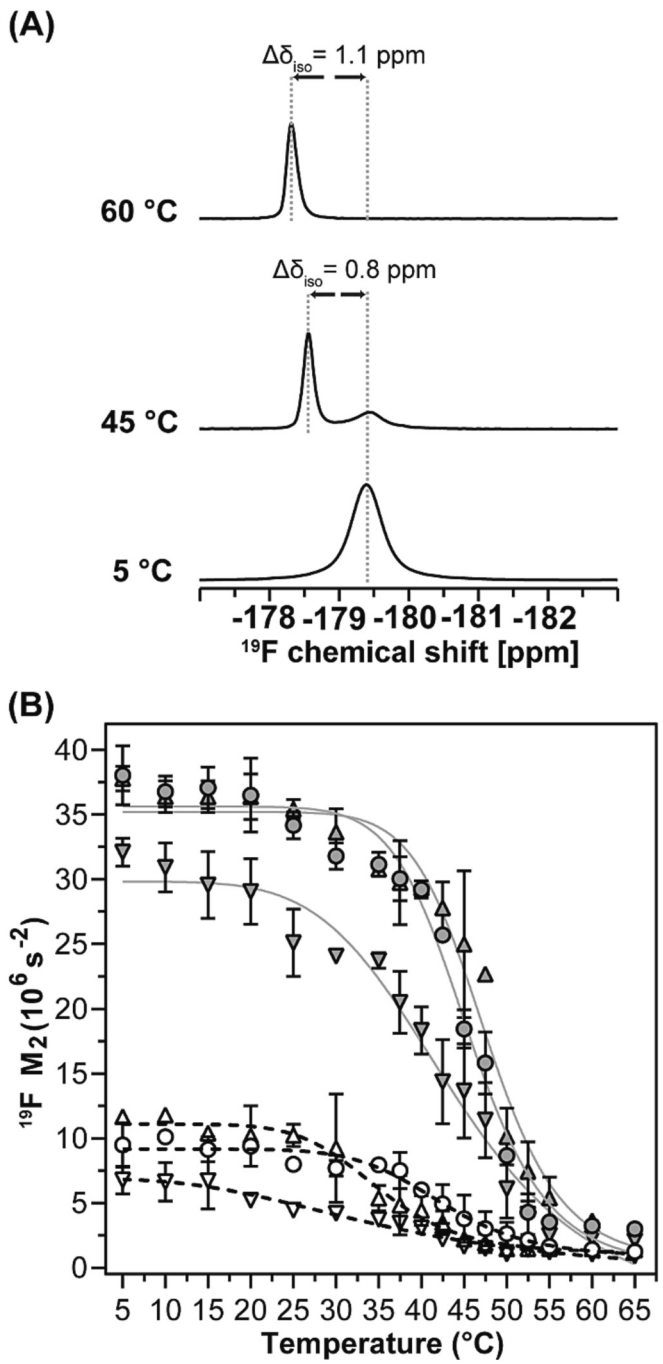

Fig. 4. (A) MAS (10 kHz) ^{19}F ssNMR spectra of DPPC/PA-F(8) model membranes, with change in isotropic chemical shift ($\Delta\delta_{iso}$) values as function of temperature. (B) Second spectral moment with standard deviation, calculated from the ^{19}F ssNMR MAS spectra (Fig. S6) of DPPC/DPPC-d_{62} with fluorinated PAs analogues at a 1:1:1 molar ratio. Experiments were carried out at different temperatures with (black, dashed line) and without (grey, solid line) ^{1}H decoupling and symbols are (○): PA-F(4), (△): PA-F(8) and (▽): PA-F(14).

Since MAS considerably enhances the signal intensity, we further evaluated the membrane dynamics in a site-resolved fashion by measuring the spin-lattice (T_1) and spin-spin relaxation (T_2) times at each position by ^{19}F ssNMR (Table S1). Both T_1 and T_2 values increased as the ^{19}F atom position moved from the headgroup region to the center

of the bilayer. The same trend was observed with increasing temperature (data not shown), confirming that T_1 and T_2 values indeed report changes in dynamics. The concomitant increase in T_1 with dynamics indicate that the correlation times of the motions contributing to longitudinal relaxation are in the nanosecond timescale, i.e. faster than the inverse of the Larmor frequency ($\tau_C < 1/\omega_0 \approx 3$ ns). Motions with this type of correlation times are most likely trans-gauche isomerisations. If such motions are affected by the interaction with AMPs, a corresponding change in T_1 should thus be observed.

3.2. Monofluorinated fatty acids to study whole cell membranes

Once the ^{19}F ssNMR methods were established in model membranes, we assessed their application to study membranes in intact cells. Early work on bacterial membranes established the possibility of labelling intact bacteria with fluorinated FAs [19,27]. Here, we focused on erythrocyte ghosts, which we had successfully labelled with deuterated PA (PA-d_{31}) in a previous study [9]. Using a similar protocol, we achieved the incorporation of MFFAs into ghosts with labelling levels up to 30 %, as determined by GC–MS (Fig. S8). Moreover, fluorescence microscopy images of the ^{19}F-labelled ghosts obtained with the lipophilic tracer FAST-DiI and the NBD-PA fluorophore, which is structurally similar to PA, show that they retain their original RBC morphology (Fig. 5A).

Fig. 5B shows static ^{19}F ssNMR spectra of RBC ghosts incorporating MFPAs at 20 °C, which are all characteristic of lipids in a lamellar phase. ^{31}P ssNMR spectra are also shown for comparison. Note that all the different phospholipid headgroups in ghosts, which contain ca. 43 % PC, 23 % phosphatidylethanolamine, 6 % phosphatidylserine and 22 % sphingomyelin, contribute to the broad ^{31}P NMR spectra [9]. As was the case in model membranes, ^{19}F spectra are characteristic of the acyl chain order at each carbon position. Indeed, the ^{19}F CSA value at the 4th position close to PA's headgroup is 7.7 ppm, which is smaller than at the 8th position (10.1 ppm). The small CSA value of 4.5 ppm at position 14 reflects the high mobility in the middle of the bilayer. As established in Section 3.1, we used the CSA values to determine the order parameter as a function of the fluorine atom position, and found S_{CF} values of 0.43, 0.56 and 0.27 for positions 4, 8 and 14, respectively. The higher order determined for PA-F(8) is in line with the characteristics expected in a membrane with a high cholesterol content, where the central portion of the acyl chains is known to be more rigid compared to the chain's beginning or end [47].

^{19}F ssNMR MAS spectra (Fig. 5B) show that the trend of the isotropic linewidth as a function of the fluorine atom position is similar to that of the CSA values. The more rigid 8th position has the broadest full width at half maximum (FWHM = 180 Hz), followed by the 4th position (158 Hz) then the more mobile 14th position (103 Hz). We further explored the membrane dynamics by monitoring the ^{19}F relaxation times of the MFFAs' isotropic resonance in ghosts (which we will refer to as P_1 peak). As reported in Table 1, T_1 values vary with the ^{19}F atom position, similarly to model DPPC membranes. Values of 328, 414 and 607 ms were respectively determined for positions 4, 8 and 14, i.e., shorter than in DPPC bilayers. This suggests that fluorinated PA probes experience an increase in motions on the nanosecond timescale when incorporated in the ghost membranes, revealing the higher fluidity of ghost membranes as compared to those formed by DPPC. T_2 values in ghosts, which range from 1.5 ms for F(4) to 2.4 ms for F(14), do not differ significantly from those determined in model membranes, implying that millisecond timescale motions are similar in these two types of bilayers. The T_2 value for PA-F(8) is the lowest (1.3 ms), consistent with the lowest FWHM value.

The isotropic peaks observed on ^{19}F ssNMR MAS spectra are sufficiently well separated to be resolved in a mixture of the three FAs, or if a triply labelled FA was prepared. The acyl chain order could then be studied in a single experiment while benefiting from the high sensitivity offered by MAS, providing that a triple labelling would not affect the membrane assembly. Altogether, our results show that both the membrane structure and dynamics are measurable by labelling whole cells such as RBC ghosts with MFPAs. Their physicochemical properties can thus be investigated, enabling the study of their interaction with membrane-active molecules.

3.3. Interaction of caerin 1.1 with ^{19}F-labelled erythrocyte ghosts

We verified the applicability of our ^{19}F ssNMR approach to study the interaction mechanism of an AMP with intact cells. To do so, we used caerin 1.1 – a 25 amino-acid cationic peptide with the following primary sequence: GLLSVLGSVAKHVLPHVVPVIAEHL-NH_2. This AMP was shown to create pores in RBC ghosts labelled with deuterated PA (PA-d_{31}) by ^{31}P and ^{2}H ssNMR in our previous work [9]. Fig. 6A-C present the static ^{19}F ssNMR spectra of the ghosts labelled at positions 4, 8 and 14, for different lipid-to-peptide (L/P) molar ratios. The ^{31}P ssNMR spectra are available in the SI (Fig. S9) for comparison. The ^{19}F spectra show the presence of a central resonance at approximately 180 ppm with a linewidth ranging from 300 to 400 Hz in the presence of caerin 1.1. Rather than resulting from small fast tumbling objects, the breadth of this line could for example indicate the presence of high-curvature regions in the ghost membranes (see below). ^{19}F CSA values decrease as a function of peptide concentration for ghosts containing PA-F(8) and PA-F(14), indicating an increased mobility at these positions. An opposite trend is observed for ghosts labelled with PA-F(4), suggesting a proximity of the AMP to the headgroup region of the membrane with local motion hindrance.

The membrane perturbing effect revealed by ^{19}F static NMR (and ^{31}P) correlates well with caerin-induced RBC leakage assays [9]. Indeed, the appearance of the isotropic peak in the ghosts and the RBC leakage occur at roughly the same L/P ratios. These observations are in good agreement with our previous work [9] as well as fluorescence microscopy images in Fig. S10, which suggest the formation of pores in the ^{19}F-labelled ghosts membrane. It should be noted that the L/P ratio refers to the total number of molecules present *in the whole sample*; the local ratio at the actual membrane is most certainly smaller due to AMP partitioning between the membrane and buffer.

Fig. 6D-F show the ^{19}F MAS ssNMR spectra of fluorinated ghosts with different concentrations of caerin 1.1. As was the case in model membranes, the anisotropic interactions are conveniently averaged by MAS even at a moderate frequency of 10 kHz. Without peptide, the area of each broad spectrum is concentrated into a single narrow line (noted P_1) with an associated increase in the S/N ratio. Interestingly, when caerin is added, an additional resonance (P_2) emerges and its intensity increases with peptide concentration. This peak is observed with all MFFA analogues. Both P_1 and P_2 resonances are best resolved when the ^{19}F atom is located at positions 8 and 14. The appearance of two isotropic peaks upon caerin addition suggests that the MFFAs are in two different environments, which we quantified by integrating P_1 and P_2 lines. As shown in Fig. 7 (Table S2), the P_2 contribution to the MAS ^{19}F ssNMR spectra is in excellent agreement with the isotropic contribution to the static ^{19}F and ^{31}P ssNMR spectra.

We then explored dynamics changes in the membrane in the presence of AMPs by measuring T_1 and T_2 relaxation times under MAS. At all fluorine atom positions, the T_1 relaxation time of the P_2 resonance is consistently shorter than that of P_1 by approximately 100 ms, suggesting that the presence of interacting caerin increases the motions on the nanosecond timescale that contribute to T_1 relaxation. On the other hand, the T_2 values are similar for P_1 and P_2. When comparing the T_1 and T_2 values of the ghosts/AMP systems with those of MFFAs incorporated in fast reorienting isotropic dodecylphosphocholine (DPC) micelles, Table 1 shows that P_2's T_1 values are slightly lower, and T_2 values are an order of magnitude smaller in the AMP-perturbed ghosts.

The presence of an isotropic peak in the static spectra, a small change in T_1 and strong reduction in T_2 have been shown, in the case of ^{31}P ssNMR, to be characteristic of high-curvature regions such as cubic or

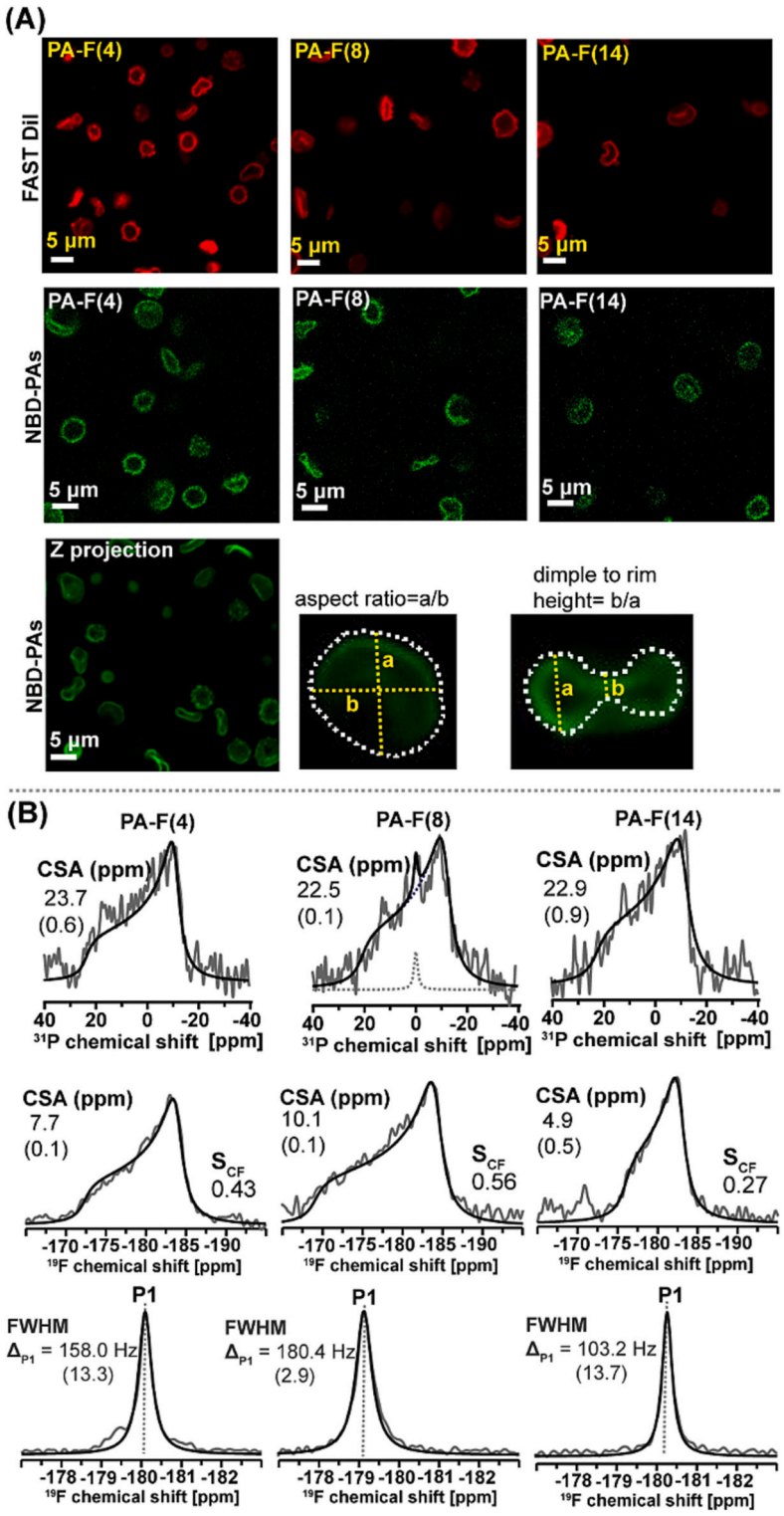

Fig. 5. (A) Confocal fluorescence microscopy images of erythrocyte ghosts labelled with monofluorinated PAs. Secondary fluorophore incorporation was achieved using lipophilic tracer FAST DiI (red) after ^{19}F labelling, NBD-PA (green) incorporation was achieved along with the ^{19}F labelling protocol. Scale bars are 5 µm and Z projection image of labelled ghosts with an average aspect ratio is indicated. (B) Static ^{31}P (top), static ^{19}F (middle) and ^{19}F MAS (10 kHz) ssNMR spectra of erythrocyte ghosts labelled with monofluorinated PAs, recorded at 293 K with ^{1}H decoupling. CSA and FWHM values are indicated, with standard deviation. Note the significant improvement in S/N ratio between ^{31}P and ^{19}F NMR. (For interpretation of the references to colour in this figure legend, the reader is referred to the web version of this article.)

Table 1
Average ^{19}F chemical shifts and ^{19}F T_1 values in different systems incorporating monofluorinated PA probes, with standard deviation. Values calculated from MAS ^{19}F ssNMR spectra recorded at 293 K with ^{1}H decoupling.

^{19}F analogue	DPC Micelles			DPPC/DPPC-d_{62}/PA			Ghosts[a] (P_1)			Ghosts + Caerin 1.1 (P_2)		
	δ_{iso} (ppm)	T_1 (ms)	T_2 (ms)	δ_{iso} (ppm)	T_1 (ms)	T_2 (ms)	δ_{iso} (ppm)	T_1 (ms)	T_2 (ms)	δ_{iso} (ppm)	T_1 (ms)	T_2 (ms)
PA-F(4)	−180.4	382 (53)	23.8 (14.6)	−180.9	611 (47)	1.7 (0.2)	−180.1	328 (27)	1.5 (0.3)	−179.7	226 (24)	1.1 (0.1)
PA-F(8)	−178.2	487 (18)	18.4 (8.1)	−179.7	760 (163)	2.2 (0.1)	−179.2	414 (4.2)	1.3 (0.4)	−178.6	310 (77)	0.9 (0.1)
PA-F(14)	−179.9	731 (10)	24.9 (5.8)	−181.3	883 (54)	2.2 (0.1)	−180.3	607 (19.1)	2.4 (0.1)	−179.9	472 (69)	1.8 (0.2)

[a] P_1 has the same isotropic chemical shift and T_1 values, without and with caerin 1.1.

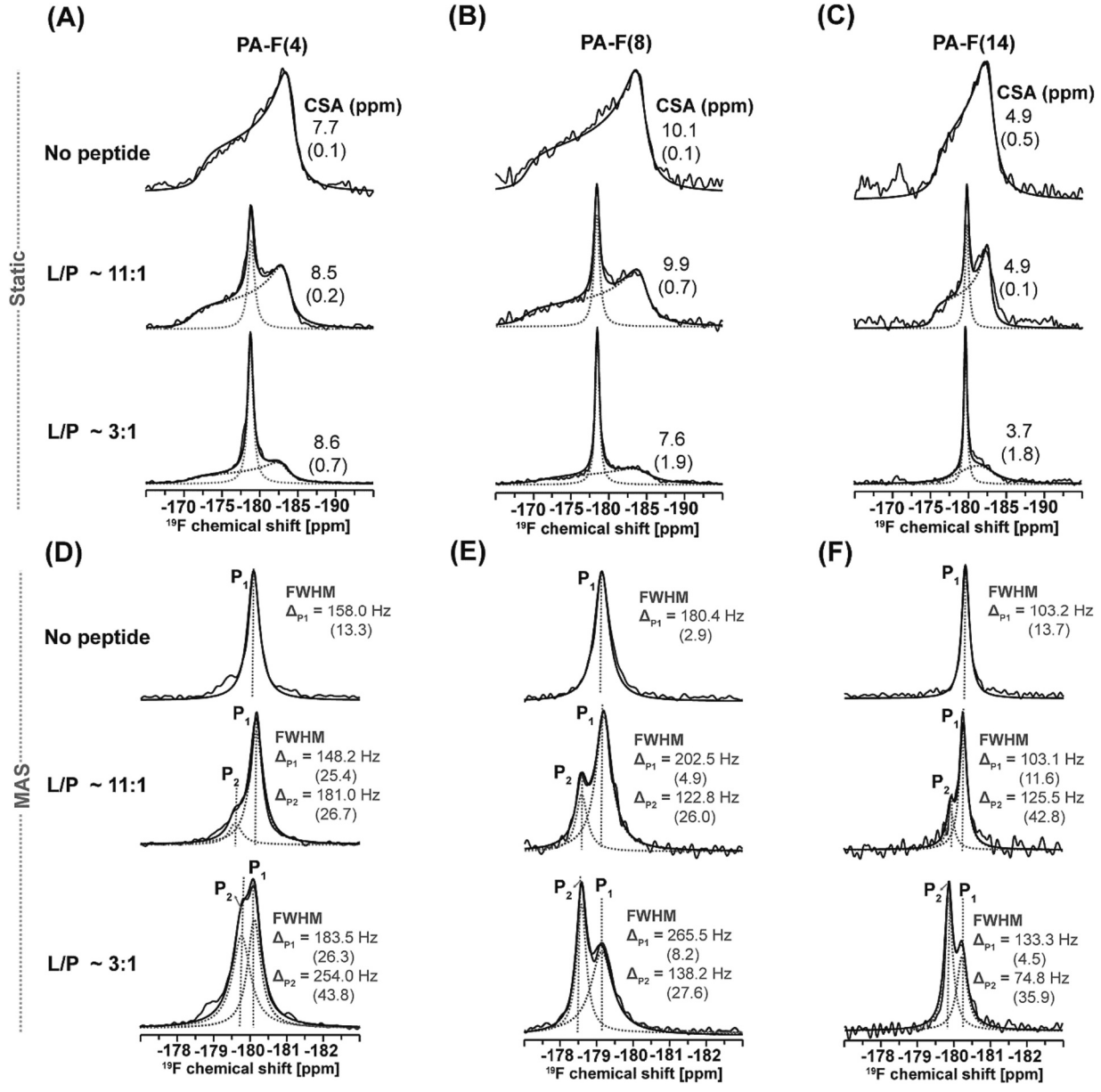

Fig. 6. Static (A-C) and MAS (D—F) ^{19}F ssNMR spectra of erythrocyte ghosts labelled with PA-F(4) (A and D), PA-F(8) (B and E) and PA-F(14) (C and F), exposed to different concentrations of caerin 1.1. Spectra were recorded at 293 K with ^{1}H decoupling. CSA and FWHM values are indicated, with standard deviation. Note the changes of linewidth with fluorine position.

hexagonal phases [48,49]. In full analogy, we thus assign the isotropic peak in our static ^{19}F spectra and P_2 peak in the MAS spectra to high-curvature regions induced by the AMP. Our NMR and microscopy results rule out a carpet mechanism, which leads to the formation of micelles. *A contrario*, the presence of high curvature regions could be due to the formation of toroidal pores for example, a result consistent with our leakage assay and fluorescence microscopy results [9]. Control experiments (not shown) rule out the possibility of hexagonal phase formation.

4. Discussion

The objective of this study was to leverage the labelling of whole

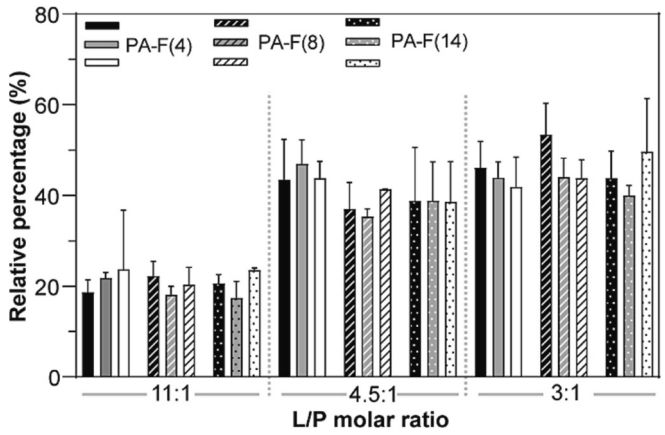

Fig. 7. Isotropic contribution in the static ^{31}P (black) and ^{19}F (grey) ssNMR spectra compared to the P_2 contribution (white) in the MAS (10 kHz) ^{19}F ssNMR spectra as a function of caerin 1.1 concentration in erythrocyte ghosts containing monofluorinated PAs.

cells with MFFAs to investigate specific interactions using ^{19}F ssNMR. Fluorine offers several key advantages, including high sensitivity, which reduces acquisition time (a critical factor for whole-cell and in vivo studies), low occurrence in biological samples, which minimizes background signals, and a broad chemical shift range, allowing for sensitivity to even minor structural changes. Fluorine is an isostere of hydrogen that alters the hydrogen bonding properties and dipole moment of the molecule in which it is incorporated [50,51]. As a consequence, fluorination can change the polarity and hydrophobicity of a molecule to an extent that will depend on the location and level of fluorination [50]. Here, we showed, as have others in similar systems, that the incorporation of MFFAs has only minor effects on the membrane structure [19,22,27], and that it can report changes in the bilayer's dynamics that are of great relevance to the study of membrane-protein interactions [19,27,33,52].

Using model DPPC membranes incorporating PA fluorinated at three different positions along the acyl chains, we established that changes in the ^{19}F CSA, isotropic chemical shift and linewidth, as well as T_1 and T_2 relaxation times, can inform on changes in the lipid bilayer dynamics. To further characterize these changes, we introduced the order parameter S_{CF} as well as M_2 measurements, similar to the widely used ^{2}H ssNMR study of perdeuterated lipids. We then showed that ^{19}F ssNMR is a valuable tool to describe the membrane state in whole erythrocyte ghosts and to monitor AMP-membrane interactions. The results obtained here using our ^{19}F ssNMR methodology are consistent with previous work reporting a pore formation mechanism for caerin, thus validating our approach.

^{19}F static spectra enabled the distinction between lamellar and non-lamellar phases with a higher sensitivity than ^{31}P ssNMR. Preliminary data also show that hexagonal phases can be identified by ^{19}F ssNMR (data not shown). In addition, ^{19}F ssNMR with appropriate labelling could replace ^{31}P ssNMR in membranes deprived of phospholipids, such as plant membranes for example. The spectra can be interpreted in terms of an order parameter reflecting the acyl chain order in a similar way to static ^{2}H ssNMR. The use of MAS, combined to the large chemical shift range of ^{19}F NMR enables distinguishing lamellar and high-curvature regions in a spectrum where anisotropic interactions are fully averaged and all the intensity is concentrated into sharp peaks. This greatly reduces the experimental time and also opens the possibility of measuring relaxation times, allowing to probe dynamical properties of the molecules.

In summary, by adequately selecting the ^{19}F position on the acyl chain, ^{19}F ssNMR can provide the same information as ^{2}H and ^{31}P ssNMR in lipid systems. Typically, knowledge of acyl chain order necessitates the measurement of anisotropic interactions such as CSA, quadrupolar couplings, or dipolar couplings [32,35]. While the simplest approach may involve studying static samples, it is conceivable to reintroduce these anisotropic interactions, thereby harnessing the advantages offered by both MAS and static spectra [32]. In this regard, the broader range of ^{19}F chemical shifts, compared to ^{31}P and even more so to ^{2}H, becomes advantageous. Additionally, information obtained from anisotropic interactions can be readily complemented by relaxation time measurements, as demonstrated in this study.

5. Conclusions

In this work, we showed how ^{19}F ssNMR is a useful tool to understand the interaction of AMPs with model membranes and, more importantly, whole cells. The incorporation of fluorinated FA probes placed at different depths in the membrane enables mapping changes in dynamics at various locations in the membrane hydrophobic core, thus complementing other biophysical methods such as ^{31}P ssNMR to describe membrane-peptide interactions. Considering its location in the middle of the acyl chain, PA-F(8) would be the preferred MFFA if a single position needs to be chosen. ^{19}F ssNMR experiments can be carried out with static samples or under MAS, with and without ^{1}H decoupling, each of these approaches having its advantages. The results presented in this work should guide the choice of a ^{19}F ssNMR experiment to investigate lipid membranes in both model and cell systems, whether it concerns membrane structure, dynamics, or a peptide mode of action. We exemplified our methodology with the study of the cationic AMP caerin 1.1 as it interacts with erythrocyte membranes. The labelling strategy presented in this work should be widely applicable to other cells such as bacteria.

CRediT authorship contribution statement

Kiran Kumar: Formal analysis, Investigation, Methodology, Validation, Visualization, Writing – original draft. **Alexandre A. Arnold:** Conceptualization, Formal analysis, Investigation, Methodology, Supervision, Validation, Writing – review & editing. **Raphaël Gauthier:** Investigation, Methodology. **Marius Mamone:** Investigation, Methodology. **Jean-François Paquin:** Investigation, Supervision, Methodology, Resources, Writing – review & editing. **Dror E. Warschawski:** Conceptualization, Formal analysis, Methodology, Supervision, Writing – review & editing. **Isabelle Marcotte:** Conceptualization, Funding acquisition, Project administration, Resources, Supervision, Writing – review & editing, Methodology.

Declaration of competing interest

The authors declare that they have no known competing financial interests or personal relationships that could have appeared to influence the work reported in this paper.

Data availability

Data will be made available on request.

Acknowledgements

This research was funded by the Natural Sciences and Engineering Research Council (NSERC) of Canada (grant RGPIN-2018–06200 to I. M.) and the Centre National de la Recherche Scientifique (UMR 7203 to D.E.W.). K.K. would like to thank the Quebec Network for Research on Protein Function, Engineering, and Applications (PROTEO) - strategic cluster of the Fonds de recherche du Québec – Nature et technologies (FRQNT) - for the award of a scholarship. The authors thank Dr. Mathew Sebastiao (Université du Québec à Montréal) for technical assistance and Pierre Audet (Université Laval) for the loan of the HFX probe.

Appendix A. Supplementary data

Supplementary data to this article can be found online at https://doi.org/10.1016/j.bbamem.2023.184269.

References

[1] M.I. Hutchings, A.W. Truman, B. Wilkinson, Antibiotics: past, present and future, Curr. Opin. Microbiol. 51 (2019) 72–80.
[2] S.B. Levy, The challenge of antibiotic resistance, Sci. Am. 278 (1998) 46–53.
[3] M. Magana, M. Pushpanathan, A.L. Santos, L. Leanse, M. Fernandez, A. Ioannidis, M.A. Giulianotti, Y. Apidianakis, S. Bradfute, A.L. Ferguson, The value of antimicrobial peptides in the age of resistance, Lancet Infect. Dis. 20 (2020) e216–e230.
[4] U. Gawde, S. Chakraborty, F.H. Waghu, R.S. Barai, A. Khanderkar, R. Indraguru, T. Shirsat, S. Idicula-Thomas, CAMPR4: a database of natural and synthetic antimicrobial peptides, Nucleic Acids Res. 51 (2023) D377–D383.
[5] K. Browne, S. Chakraborty, R. Chen, M.D. Willcox, D.S. Black, W.R. Walsh, N. Kumar, A new era of antibiotics: the clinical potential of antimicrobial peptides, Int. J. Mol. Sci. 21 (2020) 7047.
[6] C. Aisenbrey, A. Marquette, B. Bechinger, The Mechanisms of Action of Cationic Antimicrobial Peptides Refined by Novel Concepts from Biophysical Investigations, Antimicrobial Peptides: Basics for Clinical Application, 2019, pp. 33–64.
[7] N. Harmouche, B. Bechinger, Lipid-mediated interactions between the antimicrobial peptides magainin 2 and PGLa in bilayers, Biophys. J. 115 (2018) 1033–1044.
[8] E. Strandberg, A.S. Ulrich, NMR methods for studying membrane-active antimicrobial peptides, Concept. Magn. Reson. A 23 (2004) 89–120.
[9] K. Kumar, M. Sebastiao, A.A. Arnold, S. Bourgault, D.E. Warschawski, I. Marcotte, In situ solid-state NMR study of antimicrobial peptide interactions with erythrocyte membranes, Biophys. J. 121 (2022) 1512–1524.
[10] A. Naito, N. Matsumori, A. Ramamoorthy, Dynamic membrane interactions of antibacterial and antifungal biomolecules, and amyloid peptides, revealed by solid-state NMR spectroscopy, Biochim. Biophys. Acta Gen. Subj. 1862 (2018) 307–323.
[11] M. Meier, J. Seelig, Lipid and peptide dynamics in membranes upon insertion of n-alkyl-β-D-glucopyranosides, Biophys. J. 98 (2010) 1529–1538.
[12] I. Marcotte, M. Auger, Bicelles as model membranes for solid-and solution-state NMR studies of membrane peptides and proteins, Concept. Magn. Reson. A 24 (2005) 17–37.
[13] J. Pius, M.R. Morrow, V. Booth, ^{2}H solid-state nuclear magnetic resonance investigation of whole Escherichia coli interacting with antimicrobial peptide MSI-78, Biochemistry 51 (2012) 118–125.
[14] C. Tardy-Laporte, A.A. Arnold, B. Genard, R. Gastineau, M. Morançais, J.-L. Mouget, R. Tremblay, I. Marcotte, A ^{2}H solid-state NMR study of the effect of antimicrobial agents on intact *Escherichia coli* without mutating, Biochim. Biophys. Acta Biomembr. 1828 (2013) 614–622.
[15] X.L. Warnet, A.A. Arnold, I. Marcotte, D.E. Warschawski, In-cell solid-state NMR: an emerging technique for the study of biological membranes, Biophys. J. 109 (2015) 2461–2466.
[16] X.L. Warnet, M. Laadhari, A.A. Arnold, I. Marcotte, D.E. Warschawski, A ^{2}H magic-angle spinning solid-state NMR characterisation of lipid membranes in intact bacteria, Biochim. Biophys. Acta Biomembr. 1858 (2016) 146–152.
[17] P.M. Macdonald, B.D. Sykes, R.N. McElhaney, Fluorine-19 nuclear magnetic resonance studies of lipid fatty acyl chain order and dynamics in *Acholeplasma laidlawii* B membranes. A direct comparison of the effects of cis-and trans-cyclopropane ring and double-bond substituents on orientational order, Biochemistry 24 (1985) 4651–4659.
[18] B. McDonough, P.M. Macdonald, B.D. Sykes, R.N. McElhaney, Fluorine-19 nuclear magnetic resonance studies of lipid fatty acyl chain order and dynamics in *Acholeplasma laidlawii* B membranes. A physical, biochemical, and biological evaluation of monofluoropalmitic acids as membrane probes, Biochemistry 22 (1983) 5097–5103.
[19] M. Gent, P.F. Cottam, C. Ho, Fluorine-19 nuclear magnetic resonance studies of *Escherichia coli* membranes, Proc. Natl. Acad. Sci. 75 (1978) 630–634.
[20] M. Gent, P. Cottam, C. Ho, A biophysical study of protein-lipid interactions in membranes of *Escherichia coli*. Fluoromyristic acid as a probe, Biophys. J. 33 (1981) 211–223.
[21] K. Potvin-Fournier, G. Valois-Paillard, M.-C. Gagnon, T. Lefèvre, P. Audet, L. Cantin, J.-F. Paquin, C. Salesse, M. Auger, Novel approaches to probe the binding of recoverin to membranes, Eur. Biophys. J. 47 (2018) 679–691.
[22] M.-C. Gagnon, E. Strandberg, A.S. Ulrich, J.-F. Paquin, M. Auger, New insights into the influence of monofluorination on dimyristoylphosphatidylcholine membrane properties: a solid-state NMR study, Biochim. Biophys. Acta Biomembr. 1860 (2018) 654–663.
[23] K. Koch, S. Afonin, M. Ieronimo, M. Berditsch, A.S. Ulrich, Solid-state ^{19}F-NMR of peptides in native membranes, Solid State NMR (2012) 89–118.
[24] E. Strandberg, P. Wadhwani, P. Tremouilhac, U.H. Dürr, A.S. Ulrich, Solid-state NMR analysis of the PGLa peptide orientation in DMPC bilayers: structural fidelity of ^{2}H-labels versus high sensitivity of ^{19}F-NMR, Biophys. J. 90 (2006) 1676–1686.
[25] O.M. Michurin, S. Afonin, M. Berditsch, C.G. Daniliuc, A.S. Ulrich, I.V. Komarov, D. S. Radchenko, Delivering structural information on the polar face of membrane-active peptides: ^{19}F-NMR labels with a cationic side chain, Angew. Chem. 128 (2016) 14815–14819.
[26] M. Drouin, P. Wadhwani, S.L. Grage, J. Bürck, J. Reichert, S. Tremblay, M. S. Mayer, C. Diel, A. Staub, J.F. Paquin, Monofluoroalkene-Isostere as a ^{19}F NMR label for the peptide backbone: synthesis and evaluation in membrane-bound PGLa and $(KIGAKI)_3$, Chem. Eur. J. 26 (2020) 1511–1517.
[27] P.M. Macdonald, B.D. Sykes, R.N. McElhaney, Fluorine-19 NMR studies of lipid fatty acyl chain order and dynamics in *Acholeplasma laidlawii* B membranes. Fluorine-19 NMR line shape and orientational order in the gel state, Biochemistry 23 (1984) 4496–4502.
[28] M.-C. Gagnon, B. Turgeon, J.-D. Savoie, J.-F. Parent, M. Auger, J.-F. Paquin, Evaluation of the effect of fluorination on the property of monofluorinated dimyristoylphosphatidylcholines, Org. Biomol. Chem. 12 (2014) 5126–5135.
[29] M.-C. Gagnon, M. Auger, J.-F. Paquin, Progress in the synthesis of fluorinated phosphatidylcholines for biological applications, Org. Biomol. Chem. 16 (2018) 4925–4941.
[30] M.-C. Gagnon, P. Ouellet, M. Auger, J.-F. Paquin, Towards the use of monofluorinated dimyristoylphosphatidylcholines as ^{19}F NMR reporters in bacterial model membranes, J. Fluor. Chem. 206 (2018) 43–47.
[31] J. Guimond-Tremblay, M.-C. Gagnon, J.-A. Pineault-Maltais, V. Turcotte, M. Auger, J.-F. Paquin, Synthesis and properties of monofluorinated dimyristoylphosphatidylcholine derivatives: potential fluorinated probes for the study of membrane topology, Org. Biomol. Chem. 10 (2012) 1145–1148.
[32] D.E. Warschawski, A.A. Arnold, I. Marcotte, A new method of assessing lipid mixtures by ^{31}P magic-angle spinning NMR, Biophys. J. 114 (2018) 1368–1376.
[33] F. Laydevant, M. Mahabadi, P. Llido, J.-P. Bourgouin, L. Caron, A.A. Arnold, I. Marcotte, D.E. Warschawski, Growth-phase dependence of bacterial membrane lipid profile and labeling for in-cell solid-state NMR applications, Biochim. Biophys. Acta Biomembr. 1864 (2022) 183819.
[34] V. Booth, D.E. Warschawski, N.P. Santisteban, M. Laadhari, I. Marcotte, Recent progress on the application of ^{2}H solid-state NMR to probe the interaction of antimicrobial peptides with intact bacteria, Biochim. Biophys. Acta Proteins Proteom. 1865 (2017) 1500–1511.
[35] T.R. Molugu, S. Lee, M.F. Brown, Concepts and methods of solid-state NMR spectroscopy applied to biomembranes, Chem. Rev. 117 (2017) 12087–12132.
[36] B. Maraviglia, J.H. Davis, M. Bloom, J. Westerman, K.W. Wirtz, Human erythrocyte membranes are fluid down to − 5 °C, Biochim. Biophys. Acta Biomembr. 686 (1982) 137–140.
[37] A.J. Fulco, Fatty acid metabolism in bacteria, Prog. Lipid Res. 22 (1983) 133–160.
[38] M. Ibarguren, D.J. López, P.V. Escribá, The effect of natural and synthetic fatty acids on membrane structure, microdomain organization, cellular functions and human health, Biochim. Biophys. Acta Biomembr. 1838 (2014) 1518–1528.
[39] R. Koynova, B. Tenchovl, P. Quinn, P. Laggner, Structure and phase behavior of hydrated mixtures of L-dipalmitoylphosphatidylcholine and palmitic acid. Correlations between structural rearrangements, specific volume changes and endothermic events, Chem. Phys. Lipids 48 (1988) 205–214.
[40] M.E. Allen, Y. Elani, N.J. Brooks, J.M. Seddon, The effect of headgroup methylation on polymorphic phase behaviour in hydrated N-methylated phosphoethanolamine: palmitic acid membranes, Soft Matter 17 (2021) 5763–5771.
[41] K.P. Pauls, A.L. MacKay, M. Bloom, Deuterium nuclear magnetic resonance study of the effects of palmitic acid on dipalmitoylphosphatidylcholine bilayers, Biochemistry 22 (1983) 6101–6109.
[42] T. Inoue, S.-i. Yanagihara, Y. Misono, M. Suzuki, Effect of fatty acids on phase behavior of hydrated dipalmitoylphosphatidylcholine bilayer: saturated versus unsaturated fatty acids, Chem. Phys. Lipids 109 (2001) 117–133.
[43] J.H. Davis, The description of membrane lipid conformation, order and dynamics by ^{2}H-NMR, Biochim. Biophys. Acta Rev. Biomembr. 737 (1983) 117–171.
[44] D. Marquardt, F.A. Heberle, T. Miti, B. Eicher, E. London, J. Katsaras, G. Pabst, ^{1}H NMR shows slow phospholipid flip-flop in gel and fluid bilayers, Langmuir 33 (2017) 3731–3741.
[45] D.I. Fernandez, M.-A. Sani, A.J. Miles, B.A. Wallace, F. Separovic, Membrane defects enhance the interaction of antimicrobial peptides, aurein 1.2 versus caerin 1.1, Biochim. Biophys. Acta Biomembr. 1828 (2013) 1863–1872.
[46] P.M. Macdonald, B. McDonough, B.D. Sykes, R.N. McElhaney, Fluorine-19 nuclear magnetic resonance studies of lipid fatty acyl chain order and dynamics in *Acholeplasma laidlawii* B membranes. Effects of methyl-branch substitution and of trans unsaturation upon membrane acyl-chain orientational order, Biochemistry 22 (1983) 5103–5111.
[47] I. Bera, J.B. Klauda, Molecular simulations of mixed lipid bilayers with sphingomyelin, glycerophospholipids, and cholesterol, J. Phys. Chem. B 121 (2017) 5197–5208.
[48] T. Wang, S.D. Cady, M. Hong, NMR determination of protein partitioning into membrane domains with different curvatures and application to the influenza M2 peptide, Biophys. J. 102 (2012) 787–794.
[49] Y. Yang, H. Yao, M. Hong, Distinguishing bicontinuous lipid cubic phases from isotropic membrane morphologies using ^{31}P solid-state NMR spectroscopy, J. Phys. Chem. B 119 (2015) 4993–5001.
[50] B.E. Smart, Fluorine substituent effects (on bioactivity), J. Fluor. Chem. 109 (2001) 3–11.
[51] J.C. Biffinger, H.W. Kim, S.G. DiMagno, The polar hydrophobicity of fluorinated compounds, ChemBioChem 5 (2004) 622–627.
[52] M. Laadhari, A.A. Arnold, A.E. Gravel, F. Separovic, I. Marcotte, Interaction of the antimicrobial peptides caerin 1.1 and aurein 1.2 with intact bacteria by ^{2}H solid-state NMR, Biochim. Biophys. Acta Biomembr. 1858 (2016) 2959–2964.

Supplementary information for:

^{19}F solid-state NMR approaches to probe antimicrobial peptide interactions with membranes in whole cells

Kiran Kumar[1], Alexandre A. Arnold[1], Raphaël Gauthier[2], Marius Mamone[2], Jean-François Paquin[2], Dror E. Warschawski[1,3*] & Isabelle Marcotte[1*]

[1]Departement of Chemistry, Université du Québec à Montréal, P.O. Box 8888, Downtown Station, Montreal, Canada H3C 3P8

[2]PROTEO, CCVC, Département de chimie, Université Laval, 1045 Avenue de la Médecine, Québec, Québec, G1V 0A6, Canada

[3]Laboratoire des Biomolécules, LBM, CNRS UMR 7203, Sorbonne Université, École normale supérieure, PSL University, 75005 Paris, France

*Corresponding authors

Isabelle Marcotte
Tel: 1-514-987-3000 #5015
Fax: 1-514-987-4054
E-mail : *marcotte.isabelle@uqam.ca*

Dror E. Warschawski
Tel : +33 1 44 27 32 16
Fax : +33 1 44 27 62 50
E-mail : *Dror.warschawski@Sorbonne-Universite.fr*

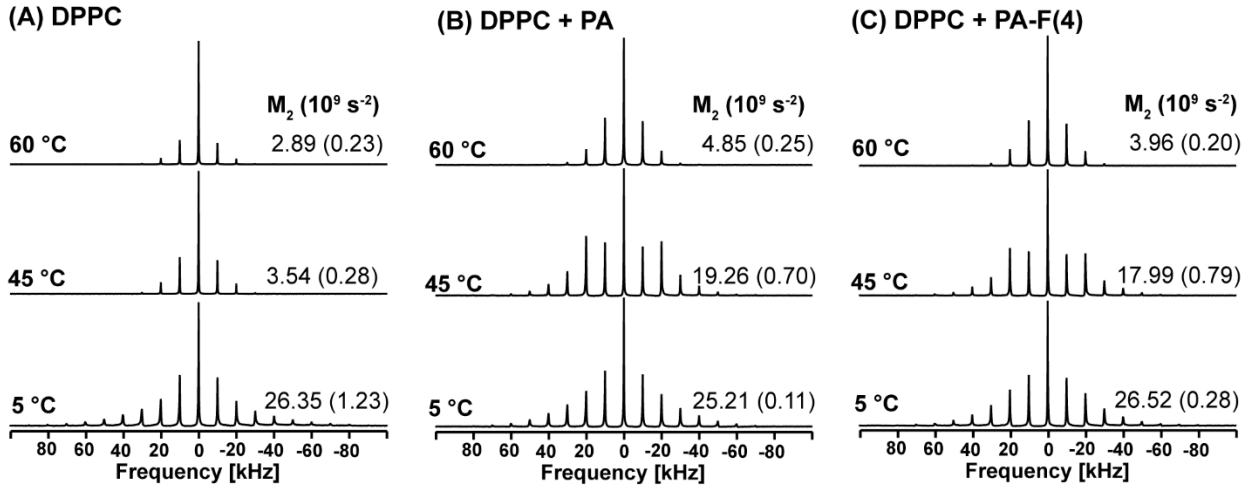

Figure S1: Representative MAS ^{2}H ssNMR spectra of **(A)** DPPC/DPPC-d_{62} (1:1), **(B)** DPPC/DPPC-d_{62}/PA (1:1:1) and **(C)** DPPC/DPPC-d_{62}/PA-F(4) as a function of temperature, recorded with 10 kHz MAS. M_2 values are indicated, with standard deviation.

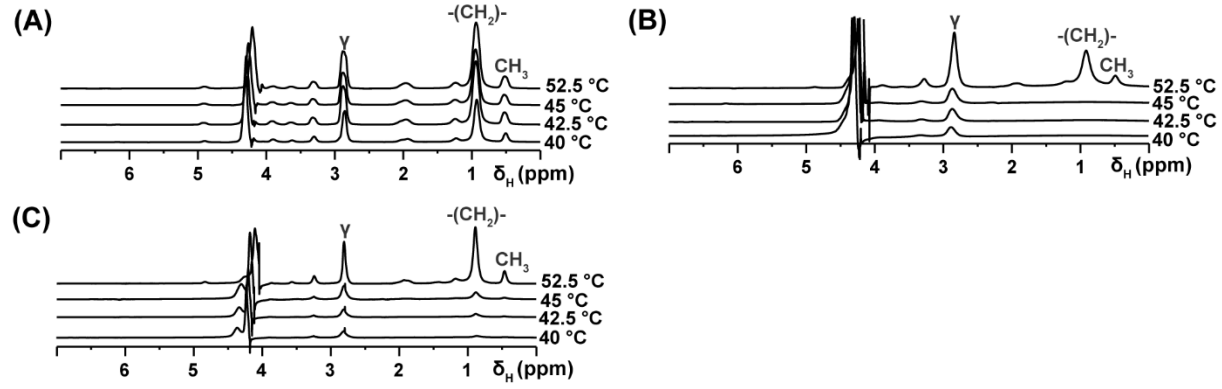

Figure S2: Representative ^{1}H ssNMR spectra of **(A)** DPPC/DPPC-d_{62} (1:1), **(B)** DPPC/DPPC-d_{62}/PA (1:1:1) and **(C)** DPPC/DPPC-d_{62}/PA-F(4) as a function of temperature, recorded with 10 kHz MAS.

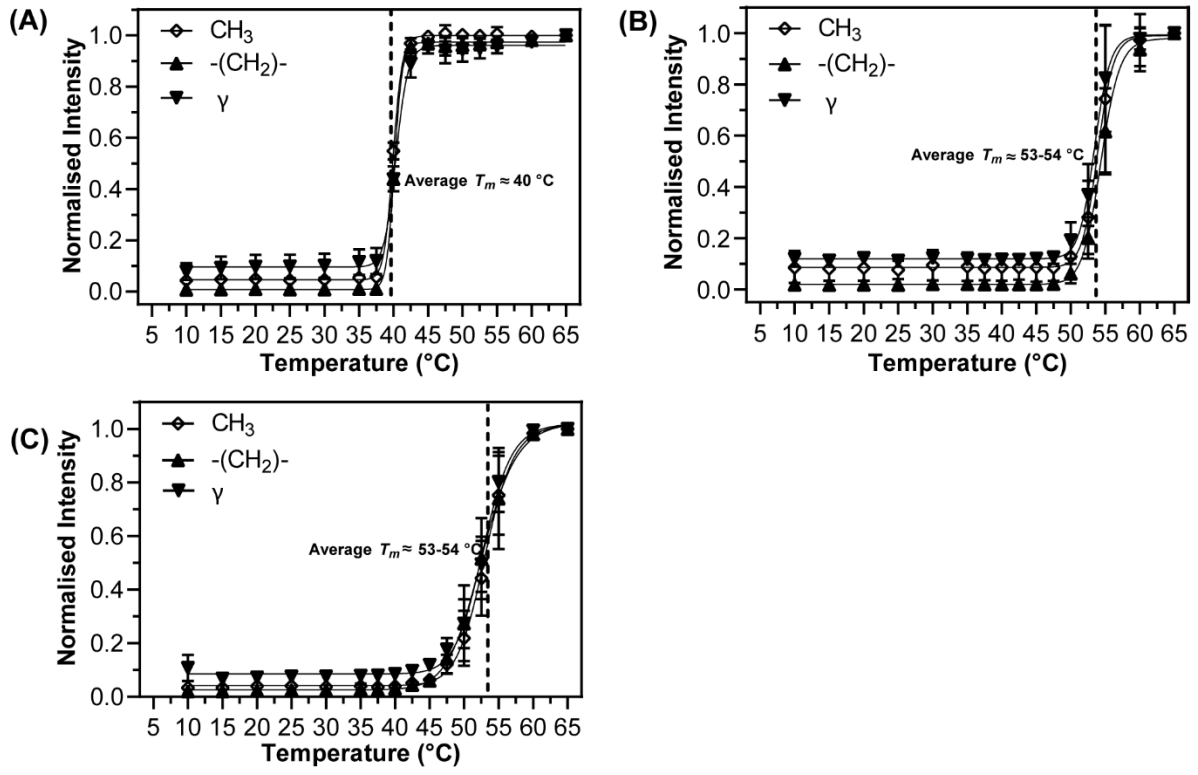

Figure S3: Determination of the gel-to-fluid phase transition temperature (T_m) of **(A)** DPPC/DPPC-d_{62} (1:1), **(B)** DPPC/DPPC-d_{62}/PA (1:1:1) and **(C)** DPPC/DPPC-d_{62}/PA-F(4) (1:1:1) through monitoring of the intensity of the methyl, methylene and γ protons from the ^{1}H ssNMR spectra, recorded with 10 kHz MAS (Fig. S2). Standard deviations are indicated.

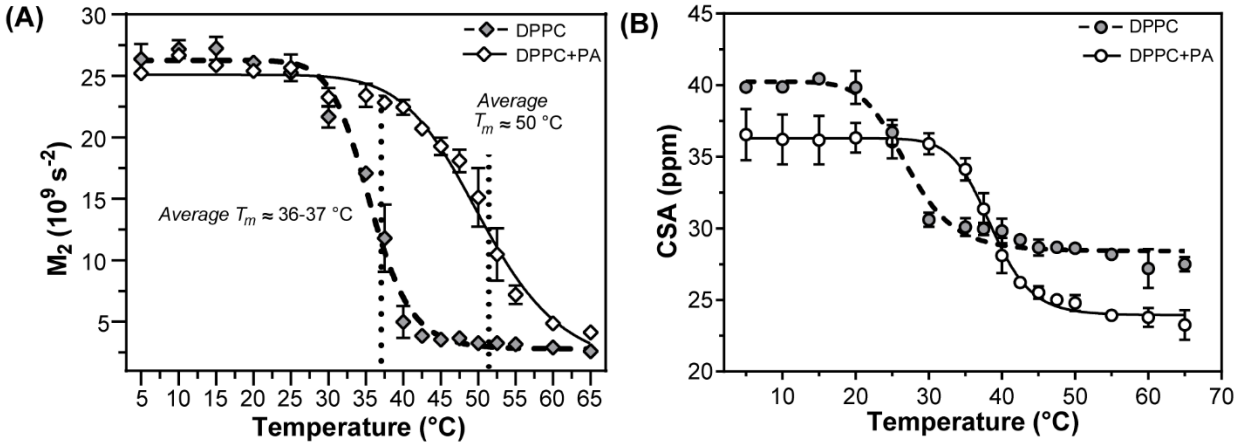

Figure S4: Temperature dependence of the M_2 and CSA values for DPPC/DPPC-d_{62} (1:1) without (dashed line) and with (solid line) protonated PA, respectively calculated from the ^{2}H (10 kHz MAS) and ^{31}P ssNMR spectra. CSA and M_2 values are indicated, with standard deviation.

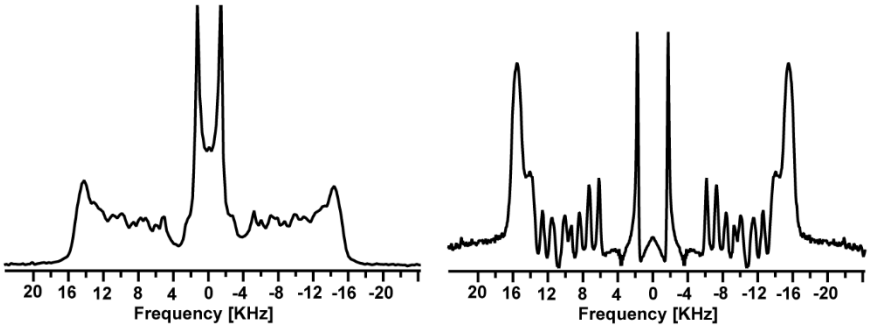

Figure S5: Representative static ^{2}H ssNMR powder-type spectrum of DPPC/DPPC-d_{62}/PA-F(4) (left) and corresponding dePaked spectrum (right) with resolved quadrupolar splittings. The spectrum wa obtained in the fluid phase (65 °C).

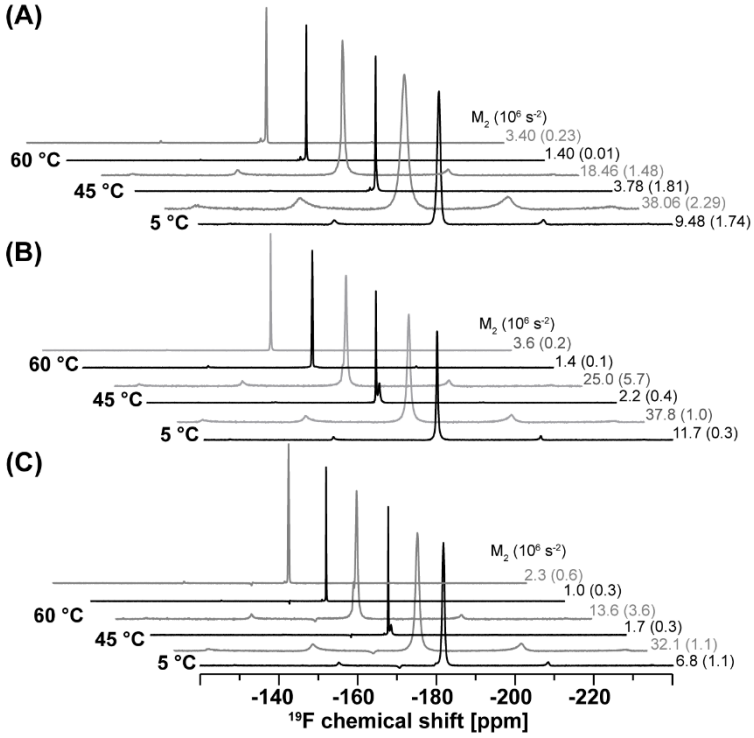

Figure S6: Representative MAS (10 kHz) ^{19}F SS-NMR spectra of DPPC/DPPC-d_{62} model membranes incorporating **(A)** PA-F(4), **(B)** PA-F(8) and **(C)** PA-F(14) at a molar ratio of 1:1:1. Spectra were recorded at different temperatures with (black) and without (grey) ^{1}H decoupling. M_2 are indicated for each spectra with standard deviation.

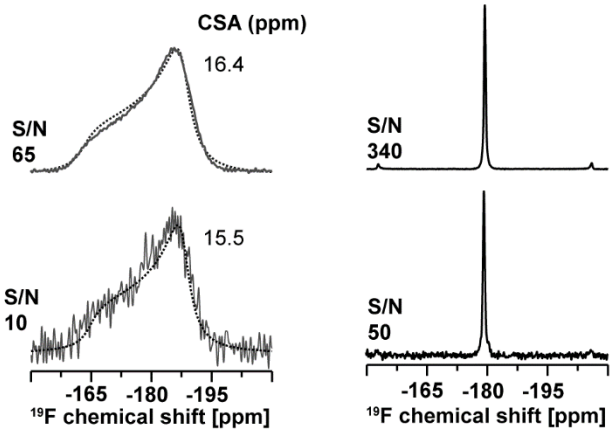

Figure S7: Static (left colum) and 10 kHz MAS (right column) 19F SS-NMR spectra with 1H decoupling of DPPC/DPPC-d62/PA-F(8) at a molar ratio of 1:1:1 at 200 mM (upper row) or 20 mM (lower row), acquired at 5 °C. Signal-to-noise (S/N) ratios are indicated, as well as simulated CSA values.

Table S1: Summary of the isotropic chemical shift (δ_{iso}) values as well as T_1 and T_2 relaxation times of monofluorinated PA analogues incorporated in DPPC/DPPC-d_{62} model membranes at a molar ratio of 1:1:1. Values are obtained from ^{1}H decoupled spectra and standard deviations are indicated.

^{19}F analogue	DPPC/DPPC-d_{62}/PA					
	278 K			293 K		
	δ_{iso} (ppm)	T_1 (ms)	T_2 (ms)	δ_{iso} (ppm)	T_1 (ms)	T_2 (ms)
PA-F(4)	-180.9	546	1.6	-180.9	611	1.7
		(5)	(0.1)		(47)	(0.2)
PA-F(8)	-179.4	652	2.2	-179.7	760	2.2
		(49)	(0.1)		(163)	(0.1)
PA-F(14)	-181.7	712	2.2	-181.3	883	2.2
		(50)	(0.2)		(54)	(0.1)

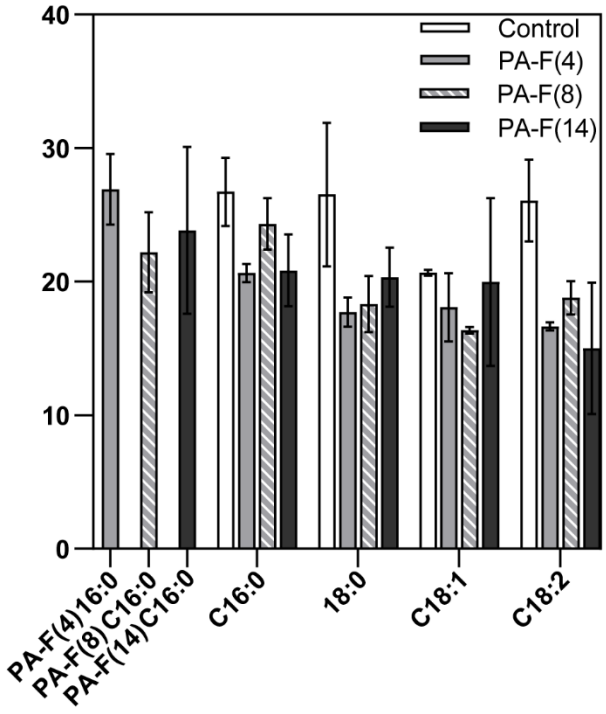

Figure S8: Fatty acyl chain profile of fluorinated erythrocyte ghosts labelled with monofluorinated PA analogues obtained by GCMS. Standard deviations are indicated.

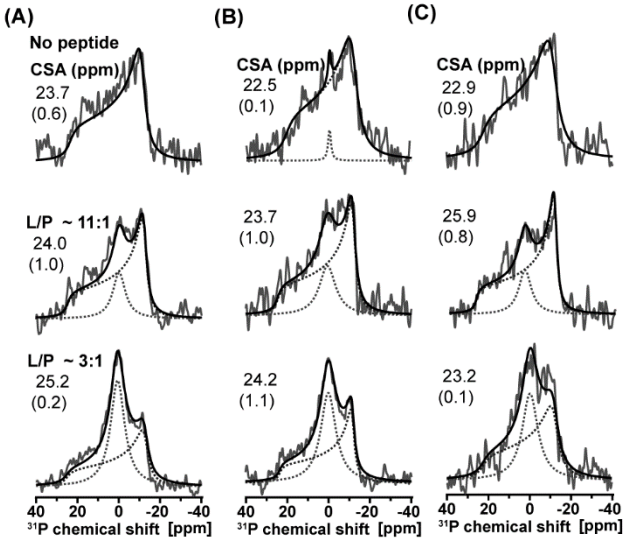

Figure S9: Static ^{31}P ssNMR spectra of erythrocyte ghosts labelled with **(A)** PA-F(4), **(B)** PA-F(8) and **(C)** PA-F(14), exposed to different concentrations of caerin 1.1. Spectra were recorded at 293 K with ^{1}H decoupling. CSA values are indicated, with standard deviation.

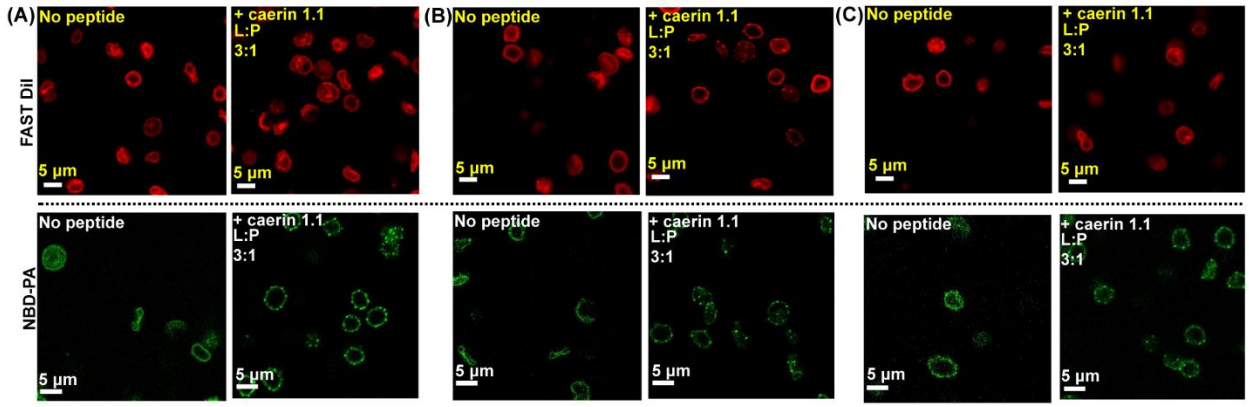

Figure S10: Confocal fluorescence microscopy images of the effect of caerin 1.1 on erythrocyte ghosts labelled **(A)** PA-F(4), **(B)** PA-F(8) and **(C)** PA-F(14). Secondary fluorophore labelling was achieved using the lipophilic tracer FAST DiI (red) after fluorination. NBD-PA (green) labelling was done along with the fluorination protocol. The corresponding L/P molar ratios are indicated, and the scale bars are 5 µm.

Table S2: Isotropic contribution on static ^{31}P and ^{19}F ssNMR spectra, and P_2 contribution from MAS (10 kHz) ^{19}F ssNMR spectra as a function of caerin 1.1 concentration. The corresponding lipid-to-peptide (L/P) molar ratio is indicated. Values are presented, with standard deviation.

	Static ^{31}P NMR			Static ^{19}F NMR			MAS ^{19}F NMR		
	PA-F(4)	PA-F(8)	PA-F(14)	PA-F(4)	PA-F(8)	PA-F(14)	PA-F(4)	PA-F(8)	PA-F(14)
L/P	Isotropic contribution (%)						P_2 contribution (%)		
11:1	18.7 (2.7)	22.3 (3.2)	20.6 (2.0)	21.8 (1.2)	18.1 (1.9)	17.4 (3.7)	23.7 (13.0)	20.4 (3.8)	23.6 (0.5)
4.5:1	43.5 (8.9)	37.0 (5.8)	38.8 (11.8)	47.0 (5.3)	35.4 (1.7)	38.9 (8.5)	43.8 (3.7)	41.4 (0.1)	38.7 (8.8)
3:1	46.1 (5.8)	53.4 (6.9)	43.8 (5.9)	43.9 (3.4)	44.0 (4.2)	40.0 (2.2)	41.9 (6.6)	43.8 (4.0)	49.7 (11.7)

General information

The following includes general experimental procedures, specific details for representative reactions, isolation and spectroscopic information for the new compounds prepared. All commercial compounds were used as received. Solvents were used as purchased unless stated as dry. THF, CH_2Cl_2 and Et_2O were purified using a Vacuum Atmospheres Inc. Solvent Purification System. All air and water sensitive reactions were carried out under argon atmosphere. Reactions were monitored by TLC on pre-coated plates (Silicycle silica gel 60 Å F254 230-240 mesh) and products were visualized under 254 nm UV light followed by staining with $KMnO_4$ or PMA. Purification by flash column chromatography was carried out on silica gel (Silicycle silica gel 60 Å, 230-400 mesh) or on Biotage® Isolera One Flash Chromatography System using the same silica gel in SNAP cartridges. All reported yields are based on weighted mass of desired product, except if stated otherwise. NMR spectra were recorded on an Agilent DD2 500 spectrometer or on a Varian Inova 400 spectrometer in the indicated solvent at 298 K. Chemical shifts for ^{1}H and ^{13}C spectra are reported on the delta scale in ppm and were referenced to TMS reference. For ^{19}F, $CFCl_3$ is used as external standard. Resonances are reported as follows: chemical shift (δ ppm), multiplicity (s = singlet, d = doublet, t = triplet, q = quartet, m = multiplet, br. s = broad signal), coupling constant (Hz), integration. High-resolution mass spectra (HRMS) were obtained on a LC/MS-TOF Agilent 6210 using electrospray ionization (ESI). Infrared spectra were recorded on an ABB MB3000 FT-IR spectrometer. Melting points were measured on a Stanford Research System OptiMelt MPA100 automated melting point apparatus and are uncorrected.

1. General procedure for the synthesis of fluorinated palmitic acids

Following synthetic pathway was inspired by our previously reported method.[1]

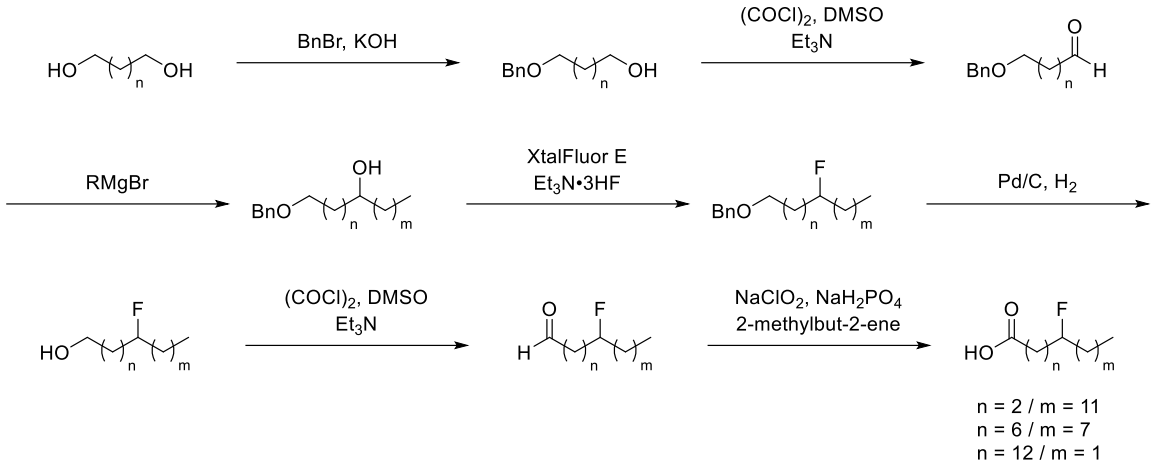

General procedure A: monobenzylation of diol

KOH (4.1 equiv) and BnBr (1 equiv) were added in 4 portions on heated diol (4.4 equiv) over 1 h. The reaction was stirred over the melting point of the diol for 3 hours. Water and EtOAc were added and the aqueous layer was extracted with EtOAC (3x). The organic layer was dried over Na_2SO_4, filtered and evaporated *in vacuo*. The crude material was purified by flash silica gel chromatography.

General procedure B: Swern oxidation to aldehyde

Anhydrous DMSO (2.4 equiv) was added dropwise to a solution of $(COCl)_2$ (1.2 equiv) in dry CH_2Cl_2 (0.2 M) cooled to -78 °C. After 20 minutes, a solution of alcohol (1 equiv) in dry CH_2Cl_2 (0.2 M) was added slowly. After 20 minutes, Et_3N (6 equiv) was added slowly. After 20 minutes, the cold bath was removed and the reaction was allowed to heat to room temperature for 1 hour. 1 M HCl was added and the mixture was stirred vigorously for 30 minutes. The aqueous layer was then extracted with CH_2Cl_2 (3x). The organic layer was washed with brine (1x), dried over Na_2SO_4, filtered and evaporated *in vacuo*. The crude material was purified by flash silica gel chromatography.

[1] Guimond-Tremblay, J.; Gagnon, M.-C.; Pineault-Maltais, J.-A.; Turcotte, V.; Auger, M.; Paquin, J.-F. *Org. Biomol. Chem.* **2012**, *10*, 1145-1148.

General procedure C: Grignard reaction

Grignard reagent solution (2 equiv) was added dropwise to a solution of aldehyde (1 equiv) in dry THF (0.2 M) cooled to 0 °C. After 15 minutes, the cool bath was removed and the reaction was allowed to heat to room temperature for 3 hours. 1 M HCl and EtOAc were added and the aqueous layer was then extracted with EtOAc (3x). The organic layer was washed with brine (1x), dried over Na_2SO_4, filtered and evaporated *in vacuo*. The crude material was purified by flash silica gel chromatography.

General procedure D: deoxofluorination and deprotection

$Et_3N{\cdot}3HF$ (2 equiv) was added dropwise to a solution of alcohol (1 equiv) and XtalFluor E (1.5 equiv) in dry CH_2Cl_2 (0.4 M) cooled to 0 °C. After 15 minutes, the cool bath was removed and the reaction was allowed to heat to room temperature for 18 hours. Saturated aqueous $NaHCO_3$ was added dropwise and the aqueous layer was extracted with CH_2Cl_2 (3x). The organic layer was washed with brine (1x), dried over Na_2SO_4, filtered and evaporated *in vacuo*. The crude material was purified by flash silica gel chromatography. The mixture of fluorination and elimination compounds was used directly for the deprotection reaction.

The mixture was dissolved in EtOAc (0.2 M) and added with Pd/C (10% wt.) in a glass reactor which was purged three times with H_2 (Parr Shaker Hydrogenation Apparatus). The pressure was then set to 50 psi of H_2 for 18 hours. The reaction mixture was filtered through a Celite pad and evaporated *in vacuo*. The crude material was purified by flash silica gel chromatography.

General procedure E: oxidation to carboxylic acid in two steps

Swern oxidation was carried out following the general procedure B, without the silica gel purification. It was followed directly by Pinnick oxidation on the crude mixture.

Sodium chlorite (2.5 equiv) was added to a solution of aldehyde (1 equiv), sodium dihydrogen phosphate dihydrate (2 equiv) and 2-methylbut-2-ene (3 equiv) in *t*-BuOH and water (3:1, 0.1 M) at room temperature. The reaction was stirred at room temperature for 90 minutes. EtOAc was added, and the aqueous layer was extracted with EtOAc (3x). The organic layer was washed with brine (1x), dried over Na_2SO_4, filtered and evaporated *in vacuo*. The crude material was purified by flash silica gel chromatography.

4-(Benzyloxy)butan-1-ol (SI-1)

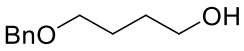

Prepared according to the general procedure A on 15.1 mmol of BnBr, using 2.2 equiv of 1,4-butanediol and 2.2 equiv of KOH. The reaction was carried out at 50 °C. The desired product (2.47 g, 13.7 mmol, 90%) was isolated as a colorless oil after purification by automated flash chromatography (15-50% EtOAc/hexanes). ^{1}H NMR (400 MHz, $CDCl_3$) δ (ppm) = 7.38–7.32 (m, 4H), 7.31–7.25 (m, 1H), 4.52 (s, 2H), 3.64 (t, *J* = 5.7 Hz, 2H), 3.52 (t, *J* = 5.9 Hz, 2H), 2.29 (br s, 1H), 1.78–1.61 (m, 2H). Data are in accordance with the one described in the literature.[2]

4-(Benzyloxy)butanal (SI-2)

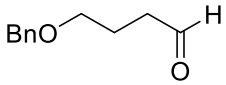

Prepared according to the general procedure B on 13.5 mmol of **SI-1**. The crude mixture was used for next step without further purification as it quickly reacts with water to generate the hydrate.

1-(Benzyloxy)hexadecan-4-ol (SI-3)

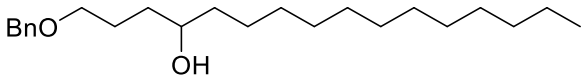

Prepared according to the general procedure C on crude mixture of **SI-2** with dodecylmagnesium bromide (1 M in Et_2O). The reaction is carried out in dry Et_2O instead of THF. The desired product (1.96 g, 5.62 mmol, 42% on 2 steps) was isolated as a white solid after purification by automated flash chromatography (10-20% EtOAc/hexanes). ^{1}H NMR (400 MHz, $CDCl_3$) δ (ppm) = 7.37–7.31 (m, 4H), 7.30–7.26 (m, 1H), 4.52 (s, 2H), 3.64–3.55 (m, 1H), 3.51 (t, *J* = 6.0 Hz, 2H), 2.22 (br s, 1H), 1.78–1.40 (m, 6H), 1.33–1.23 (m, 20H), 3.51 (t, *J* = 6.9 Hz, 3H). Data are in accordance with the one described in the literature.[3]

[2] Crimmins, M. T.; DeBaillie, A. C. *J. Am. Chem. Soc.* **2006**, *128*, 4936-4937.
[3] Liu, R.-C.; Wei, J.-H.; Wei, B.-G.; Lin, G.-Q. *Tetrahedron Asymmetry* **2008**, *19*, 2731-2734.

4-Fluorohexadecan-1-ol (SI-4)

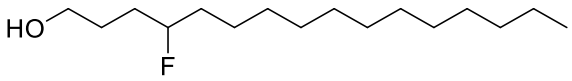

Prepared according to the general procedure D on 5.61 mmol of **SI-3**. The first purification was done by automated flash chromatography (0-5% EtOAc/hexanes). The desired product (180 mg, 0.691 mmol, 18% on 2 steps) was isolated as a white solid after purification by automated flash chromatography (5-15% EtOAc/hexanes). Mp: 57.2–58.9 °C; FT-IR ν (cm^{-1}) = 3273, 2916, 2847, 1063; ^{1}H NMR (500 MHz, $CDCl_3$) δ (ppm) = 4.60–4.42 (m, 1H), 3.69 (br. s, 3H), 1.79–1.58 (m, 5H), 1.58–1.40 (m, 2H), 1.39–1.22 (m, 20H), 0.88 (t, J = 6.9 Hz, 3H); ^{13}C NMR (126 MHz, $CDCl_3$) δ (ppm) = 94.5 (d, J_{C-F} = 166.9 Hz), 62.7, 35.2 (d, J_{C-F} = 20.9 Hz), 31.9, 31.5 (d, J_{C-F} = 21.3 Hz), 29.68, 29.65, 29.57, 29.54, 29.49, 29.36, 28.5 (d, J_{C-F} = 3.7 Hz), 25.1 (d, J_{C-F} = 4.7 Hz), 22.7, 14.1; ^{19}F NMR (470 MHz, $CDCl_3$) δ (ppm) = -179.9 – -180.3 (m, 1F); HRMS (ESI-TOF) m/z calcd for $C_{16}H_{37}FNO$ $[M+NH_4]^+$ 278.2854; found 278.2858.

4-Fluorohexadecanoic acid / PA-4(F)

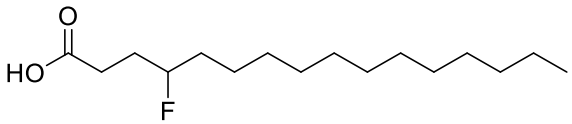

Prepared according to the general procedure E on 0.680 mmol of **SI-4** with. The desired product (77 mg, 0.281 mmol, 41% on 2 steps) was isolated as a white solid after purification by automated flash chromatography (15-50% EtOAc/hexanes). Mp: 69.5–71.4 °C; FT-IR ν (cm^{-1}) = 2916, 2849, 2737, 1699, 1296, 943; ^{1}H NMR (500 MHz, $CDCl_3$) δ (ppm) = 10.98 (br. s, 1H), 4.51 (dtt, J = 49.4, 8.0, 4.1 Hz, 1H), 2.61–2.45 (m, 2H), 2.01–1.85 (m, 2H), 1.71–1.34 (m, 4H), 1.33–1.23 (m, 18H), 0.88 (t, J = 7.0 Hz, 3H); ^{13}C NMR (126 MHz, $CDCl_3$) δ (ppm) = 178.0, 93.3 (d, J_{C-F} = 168.3 Hz), 35.1 (d, J_{C-F} = 20.5 Hz), 31.9, 30.0 (d, J_{C-F} = 21.4 Hz), 29.67, 29.64, 29.55, 29.50, 29.42, 29.36, 25.0 (d, J_{C-F} = 4.7 Hz), 22.7, 14.1; ^{19}F NMR (470 MHz, $CDCl_3$) δ (ppm) = -182.8 – -183.1 (m, 1F); HRMS (ESI-TOF) m/z calcd for $C_{16}H_{30}FO_2$ $[M-H]^-$ 273.2235; found 273.2237.

8-(Benzyloxy)octan-1-ol (SI-5)

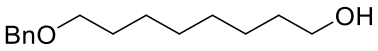

Prepared according to the general procedure A on 12.1 mmol of BnBr, using 1,8-octanediol. The reaction was carried out at 80 °C. The desired product (2.16 g, 9.14 mmol, 75%) was isolated as a colorless oil after purification by automated flash chromatography (20-50% EtOAc/hexanes). ^{1}H NMR (500 MHz, $CDCl_3$) δ (ppm) = 7.38–7.32 (m, 4H), 7.30–7.26 (m, 1H), 4.50 (s, 2H), 3.63 (t, *J* = 6.7 Hz, 2H), 3.46 (t, *J* = 6.6 Hz, 2H), 1.65–1.52 (m, 4H), 1.40–1.28 (m, 8H). Data are in accordance with the one described in the literature.[4]

8-(Benzyloxy)octanal (SI-6)

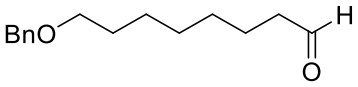

Prepared according to the general procedure B on 9.14 mmol of **SI-5**. The desired product (1.77 g, 7.55 mmol, 83%) was isolated as a colorless oil after purification by automated flash chromatography (0-10% EtOAc/hexanes). ^{1}H NMR (400 MHz, $CDCl_3$) δ (ppm) = 9.76 (t, *J* = 1.8 Hz, 1H), 7.39–7.30 (m, 4H), 7.31–7.26 (m, 1H), 4.50 (s, 2H), 3.46 (t, *J* = 6.6 Hz, 2H), 2.41 (td, *J* = 7.4, 1.9 Hz, 2H), 1.67–1.57 (m, 4H), 1.43–1.28 (m, 6H). Data are in accordance with the one described in the literature.[5]

1-(Benzyloxy)hexadecan-8-ol (SI-7)

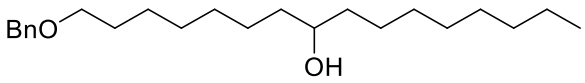

Prepared according to the general procedure C on 7.55 mmol of **SI-6** with octylmagnesium bromide (2 M in THF). The desired product (2.07 g, 5.94 mmol, 79%) was isolated as a white solid after purification by automated flash chromatography (0-10% EtOAc/hexanes). Mp: 39.8–41.8 °C; FT-IR ν (cm^{-1}) = 3266, 2970, 1695, 1300, 1215, 949, 698; ^{1}H NMR (400 MHz, $CDCl_3$) δ (ppm) = 7.37–7.32 (m, 4H), 7.31–7.25 (m, 1H), 4.50 (s, 2H), 3.58 (br. s, 1H), 3.46 (t, *J* = 6.6 Hz, 2H), 1.66–1.54 (m, 2H), 1.47–1.23 (m, 25H), 0.88 (t, *J* = 6.8 Hz, 3H); ^{13}C NMR (126 MHz, $CDCl_3$) δ (ppm)

[4] Gao, X.; Hall, D. G. *J. Am. Chem. Soc.* **2005**, *127*, 1628-1629
[5] Madda, J.; Khandregula, S.; Bandari, S. K.; Kommu, N.; Yadav, J. S. *Tetrahedron Asymmetry* **2014**, *25*, 1494-1500.

= 138.7, 128.4, 127.6, 127.5, 72.9, 72.0, 70.5, 37.53, 37.48, 31.9, 29.8, 29.74, 29.66, 29.6, 29.5, 29.3, 26.2, 25.7, 25.6, 22.7, 14.1; HRMS (ESI-TOF) m/z calcd for $C_{23}H_{41}O_2$ $[M+H]^+$ 349.3101; found 349.3112.

8-Fluorohexadecan-1-ol (SI-8)

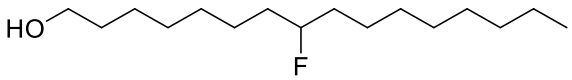

Prepared according to the general procedure D on 5.94 mmol of **SI-7**. The first purification was done by automated flash chromatography (0-5% EtOAc/hexanes). The desired product (329 mg, 1.26 mmol, 21% on 2 steps) was isolated as a white solid after purification by automated flash chromatography (5-15% EtOAc/hexanes). Mp: 54.0–54.9 °C; FT-IR ν (cm^{-1}) = 3265, 2918, 2849, 1472, 1128, 1063; ^{1}H NMR (500 MHz, $CDCl_3$) δ (ppm) = 4.45 (dtt, J = 49.1, 7.9, 3.9 Hz, 1H), 3.64 (t, J = 6.7 Hz, 2H), 1.67–1.42 (m, 8H), 1.40–1.22 (m, 19H), 0.88 (t, J = 6.8 Hz, 3H); ^{13}C NMR (126 MHz, $CDCl_3$) δ (ppm) = 94.6 (d, J_{C-F} = 166.4 Hz), 63.1, 35.2 (d, J_{C-F} = 20.9 Hz), 35.1 (d, J_{C-F} = 20.9 Hz), 32.8, 31.9, 29.53, 29.51, 29.46, 29.32, 29.25, 25.7, 25.14 (d, J_{C-F} = 4.4 Hz), 25.07 (d, J_{C-F} = 4.6 Hz), 22.7, 14.1; ^{19}F NMR (470 MHz, $CDCl_3$) δ (ppm) = -179.8 – -180.2 (m, 1F); HRMS (ESI-TOF) m/z calcd for $C_{16}H_{37}FNO$ $[M+NH_4]^+$ 278.2854; found 278.2861

8-Fluorohexadecanoic acid /PA-F(8)

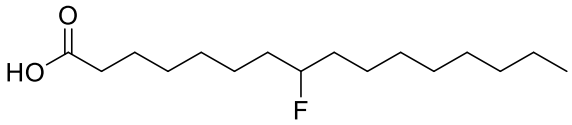

Prepared according to the general procedure E on 1.20 mmol of **SI-8** with. The desired product (211 mg, 0.769 mmol, 64% on 2 steps) was isolated as a white solid after purification by automated flash chromatography (20-40% EtOAc/hexanes). Mp: 65.4–68.2 °C; FT-IR ν (cm^{-1}) = 2916, 2849, 2728, 1701, 1472, 1296, 943; ^{1}H NMR (500 MHz, $CDCl_3$) δ (ppm) = 11.11 (br. s, 1H), 4.45 (dtt, J = 48.9, 7.8, 3.8 Hz, 1H), 2.36 (t, J = 7.5 Hz, 2H), 1.69–1.41 (m, 8H), 1.40–1.22 (m, 16H), 0.88 (t, J = 6.9 Hz, 3H); ^{13}C NMR (101 MHz, $CDCl_3$) δ (ppm) = 179.5, 94.5 (d, J_{C-F} = 166.5 Hz), 35.2 (d, J_{C-F} = 20.9 Hz), 35.1 (d, J_{C-F} = 21.0 Hz), 33.9, 31.9, 29.52, 29.51, 29.3, 29.1, 28.9, 25.1 (d, J_{C-F} = 4.6 Hz), 25.0 (d, J_{C-F} = 4.5 Hz), 24.6, 22.7, 14.1; ^{19}F NMR (470 MHz, $CDCl_3$) δ (ppm) = -179.9 – -180.5 (m, 1F); HRMS (ESI-TOF) m/z calcd for $C_{16}H_{30}FO_2$ $[M-H]^-$ 273.2235; found 273.2237.

14-(Benzyloxy)tetradecan-1-ol (SI-9)

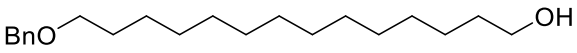

Prepared according to the general procedure A on 3.03 mmol of BnBr, using 1,14-tetradecanediol. The reaction was carried out at 110 °C. The desired product (515 mg, 1.61 mmol, 53%) was isolated as a white solid after purification by column flash chromatography (20% EtOAc/hexanes). ^{1}H NMR (500 MHz, $CDCl_3$) δ (ppm) = 7.36–7.33 (m, 4H), 7.30–7.25 (m, 1H), 4.50 (s, 2H), 3.63 (t, *J* = 6.7 Hz, 2H), 3.46 (t, *J* = 6.7 Hz, 2H), 1.66–1.51 (m, 4H), 1.39–1.23 (m, 20H). Data are in accordance with the one described in the literature.[6]

14-(Benzyloxy)tetradecanal (SI-10)

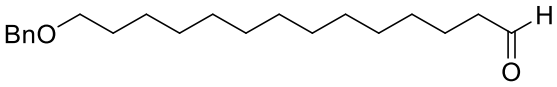

Prepared according to the general procedure B on 3.56 mmol of **SI-9**. The desired product (940 mg, 2.95 mmol, 83%) was isolated as an oily solid after purification by automated flash chromatography (0-5% EtOAc/hexanes). FT-IR ν (cm^{-1}) = 2920, 2851, 1701, 1653, 1200, 667; ^{1}H NMR (500 MHz, $CDCl_3$) δ (ppm) = 9.76 (t, *J* = 1.9 Hz, 1H), 7.36–7.32 (m, 4H), 7.30–7.25 (m, 1H), 4.50 (s, 2H), 3.46 (t, *J* = 6.7 Hz, 2H), 2.42 (td, *J* = 7.4, 1.9 Hz, 2H), 1.66–1.58 (m, 4H), 1.39–1.23 (m, 18H); ^{13}C NMR (126 MHz, $CDCl_3$) δ (ppm) = 203.0, 138.7, 128.3, 127.6, 127.6, 72.9, 70.5, 43.9, 29.8, 29.60, 29.58 29.56, 29.5, 29.42, 29.36, 29.2, 26.2, 22.1; HRMS (ESI-TOF) m/z calcd for $C_{21}H_{35}O_2$ $[M+H]^+$ 319.2632; found 319.2647.

16-(Benzyloxy)hexadecan-3-ol (SI-11)

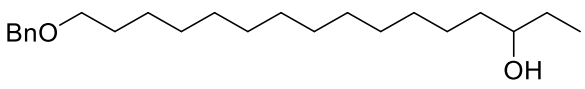

Prepared according to the general procedure C on 2.95 mmol of **SI-10** with ethylmagnesium chloride (2 M in THF). The desired product (841 mg, 2.41 mmol, 82%) was isolated as a white solid after purification by automated flash chromatography (0-10% EtOAc/hexanes). Mp: 40.5–42.5 °C; FT-IR ν (cm^{-1}) = 2918, 2851, 1456, 1103, 696; ^{1}H NMR (500 MHz, $CDCl_3$) δ (ppm) =

[6] Muller, T.; Coowar, D.; Hanbali, M.; Heuschling, P.; Luu, B. *Tetrahedron* **2006**, *62*, 12025-12040.

7.38–7.30 (m, 4H), 7.31–7.24 (m, 1H), 4.50 (s, 2H), 3.51 (br. s, 1H), 3.46 (t, *J* = 6.7 Hz, 2H), 1.65–1.58 (m, 2H), 1.57–1.22 (m, 25H), 0.94 (t, *J* = 7.5 Hz, 3H); ^{13}C NMR (126 MHz, $CDCl_3$) δ (ppm) = 138.7, 128.3, 127.6, 127.5, 73.3, 72.9, 70.5, 37.0, 30.1, 29.8, 29.7, 29.64, 29.61, 29.60, 29.5, 26.2, 25.7, 9.9; HRMS (ESI-TOF) m/z calcd for $C_{23}H_{41}O_2$ $[M+H]^+$ 349.3101; found 349.3113.

14-Fluorohexadecan-1-ol (SI-12)

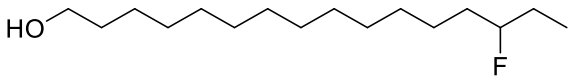

In a glass round-bottom flask, Deoxo-Fluor® (2,7 M in toluene, 1.3 mL, 3.51 mmol, 1.3 equiv) was added dropwise to a solution of **SI-11** (961 mg, 2.76 mmol, 1 equiv) in dry CH_2Cl_2 (14 mL, 0.2 M) cooled to 0 °C. After 10 minutes, the cool bath was removed and the reaction was allowed to heat to room temperature for 3 hours. Saturated aqueous $NaHCO_3$ was added dropwise and the aqueous layer was extracted with CH_2Cl_2 (3x). The organic layer was washed with brine (1x), dried over Na_2SO_4, filtered and evaporated *in vacuo*. The crude material was purified by flash silica gel chromatography (0-5% EtOAc/hexanes). The mixture of fluorination and elimination compounds was used directly for the deprotection reaction.

The mixture was dissolved in EtOAc (5 mL, 0.55 M) and added with Pd/C (97 mg, 10% wt.) in a glass reactor which was purged three times with H_2 (Parr Shaker Hydrogenation Apparatus). The pressure was then set to 50 psi of H_2 for 19 hours. The reaction mixture was filtered through a Celite pad and evaporated *in vacuo*. The desired product (193 mg, 0.741 mmol, 27% on 2 steps) was isolated as a white solid after purification by automated flash chromatography (0-15% EtOAc/hexanes). Mp: 51.0–52.7 °C; FT-IR ν (cm^{-1}) = 3313, 3232, 2916, 2849, 1464, 1063, 926, 719; ^{1}H NMR (500 MHz, $CDCl_3$) δ (ppm) = 4.49–4.31 (m, 1H), 3.64 (td, *J* = 6.2, 5.8 Hz, 2H), 1.68–1.53 (m, 6H), 1.52–1.41 (m, 2H), 1.38–1.24 (m, 18H), 1.23–1.20 (m, 1H), 0.96 (t, *J* = 7.4 Hz, 3H); ^{13}C NMR (126 MHz, $CDCl_3$) δ (ppm) = 95.9 (d, J_{C-F} = 166.6 Hz), 63.3, 34.8 (d, J_{C-F} = 20.9 Hz), 33.0, 29.77, 29.75, 29.73, 29.71, 29.69, 29.67, 29.6, 28.2 (d, J_{C-F} = 21.5 Hz), 25.9, 25.3 (d, J_{C-F} = 4.7 Hz), 9.6 (d, J_{C-F} = 5.8 Hz); ^{19}F NMR (470 MHz, $CDCl_3$) δ (ppm) = -181.2 (dtt, *J* = 48.0, 29.0, 18.3 Hz, 1F); HRMS (ESI-TOF) m/z calcd for $C_{16}H_{37}FNO$ $[M+NH_4]^+$ 278.2854; found 278.2854.

14-Fluorohexadecanoic acid /PA-F(14)

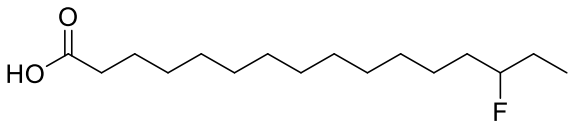

Prepared according to the general procedure E on 0.726 mmol of **SI-12** with. The desired product (98 mg, 0.357 mmol, 49% on 2 steps) was isolated as a white solid after purification by automated flash chromatography (15-40% EtOAc/hexanes). Mp: 72.9–74.5 °C; FT-IR ν (cm^{-1}) = 2912, 2849, 2635, 1697, 1472, 1439, 1211, 939; ^{1}H NMR (500 MHz, $CDCl_3$) δ (ppm) = 10.98 (br. s, 1H), 4.50–4.30 (m, 1H), 2.35 (t, *J* = 7.5 Hz, 2H), 1.67–1.41 (m, 7H), 1.37–1.24 (m, 18H), 0.96 (t, *J* = 7.4 Hz, 3H); ^{13}C NMR (101 MHz, $CDCl_3$) δ (ppm) = 179.5, 95.9 (d, J_{C-F} = 166.8 Hz), 34.8 (d, J_{C-F} = 20.9 Hz), 34.1, 29.74, 29.71, 29.70, 29.68, 29.67, 29.4, 29.2, 28.2 (d, J_{C-F} = 21.5 Hz), 25.3 (d, J_{C-F} = 4.5 Hz), 24.8, 9.6 (d, J_{C-F} = 5.8 Hz); ^{19}F NMR (470 MHz, $CDCl_3$) δ (ppm) = -181.2 (dtt, *J* = 47.7, 28.8, 18.3 Hz, 1F); HRMS (ESI-TOF) m/z calcd for $C_{16}H_{30}FO_2$ $[M-H]^-$ 273.2235; found 273.2239.